Inversion of seismic data for assessing fluid replacement in the Nisku Formation

Patricia E. Gavotti and Don C. Lawton

ABSTRACT

The seismic response of the Nisku Formation in Alberta was evaluated in terms of its impedance variations with the surrounding formations. The methodology compares the effect of using a dataset processed with different approaches in an inversion study. These approaches are based on a previously conditioned dataset with a conventional processing sequence (a) versus a new specialized processing sequence (b) focused on attaining coherent noise without compromising low-frequency signal. A model-based inversion was performed with these datasets. In both cases, the inverted impedance showed good results at the well location and yielded a similar general trend and lateral variations. The inverted impedance in case b) showed a broadband result possibly related with the presence of more low frequency content in the seismic data. In case (a) the result yielded a cleaner section and the units look more continuous without much lateral variation.

A 2D seismic modelling was undertaken to simulate a CO_2 injection scenario in the Nisku Formation. The time-lapse study was performed by comparing seismic amplitudes and impedance changes before and after the CO_2 injection. The post-injection seismic section shows a time delay of 1.8 ms of the basal reservoir reflector and amplitude change of ~30% with respect to the baseline case. After performing the inversion, a decrease in the impedance values of ~7% is observed in the post-injection scenario.

PROJECT PIONEER DATA

Several seismic feasibility studies have been undertaken in the Wabamun Lake area for determining the suitability of injecting CO_2 in some of the geological formations of that area. Project Pioneer was planning to capture one million tonnes of CO_2 annually at its Keephills 3 coal-fired power plant that would have been used for EOR opportunities in the Pembina Oil Field, or transported by pipeline to the sequestration site to be injected approximately 2 km underground into the Nisku Formation, a Devonian saline aquifer (TransAlta 2012: http://www.transalta.com/newsroom/feature-articles/2013-05-24/project-pioneer-publishes-its-final-report-pioneer-still-sharin). The project was cancelled in April 2012 (Project Pioneer, 2012: http://www.projectpioneer.ca/) but the information is available as a source of reference and the affiliation between the CREWES Project with Carbon Management Canada (CMC) allows the possibility of having access to the data for further analysis.

The study area is located in the Western Canada Sedimentary Basin (WCSB), approximately 70 km west of Edmonton, where the Wabamun Area CO_2 Sequestration Project (WASP) study was undertaken and Project Pioneer was planned to be built at the Keephills 3 power station (Figure 1).

The seismic data for this project was provided by TransAlta Corporation (TransAlta) and he well log information was provided by Schlumberger. Figures 2 and 3 show the seismic data used in this project from, a) previous processed CDP stacked and b) new processed stacked.

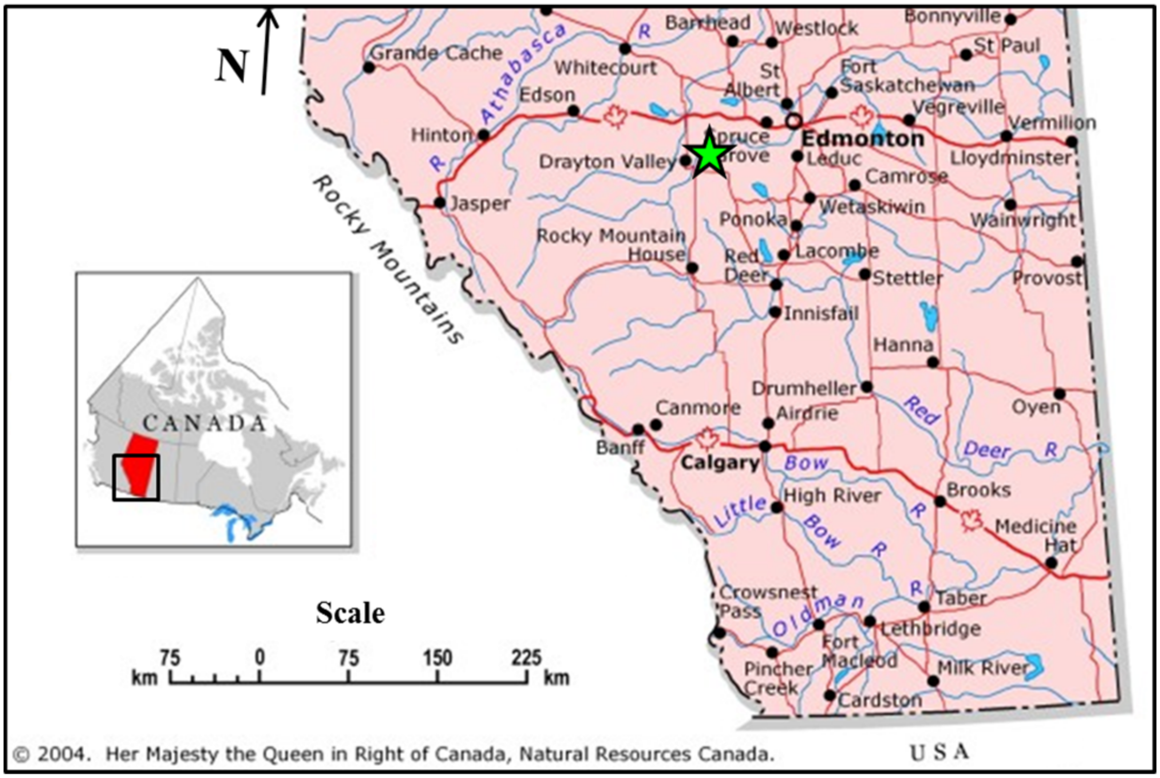

FIG. 1. Location of study area in Alberta, Canada. Project Pioneer (green star) (modified from Natural Resources Canada, 2013).

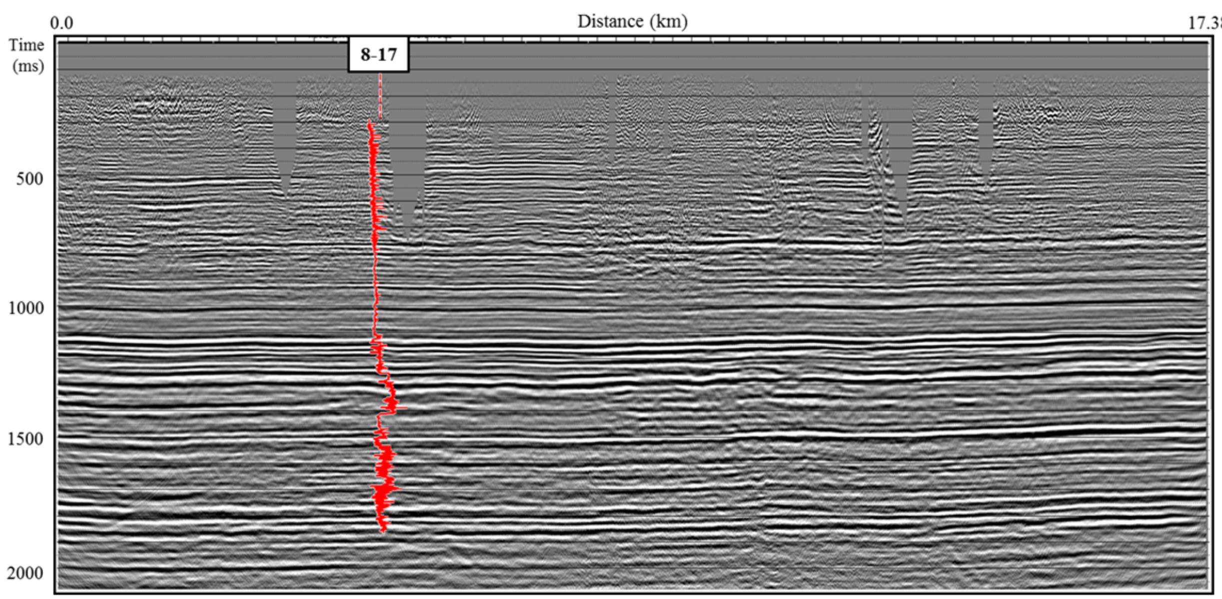

FIG. 2. Highvale stacked section from previous processing. Well 8-17 is also displayed.

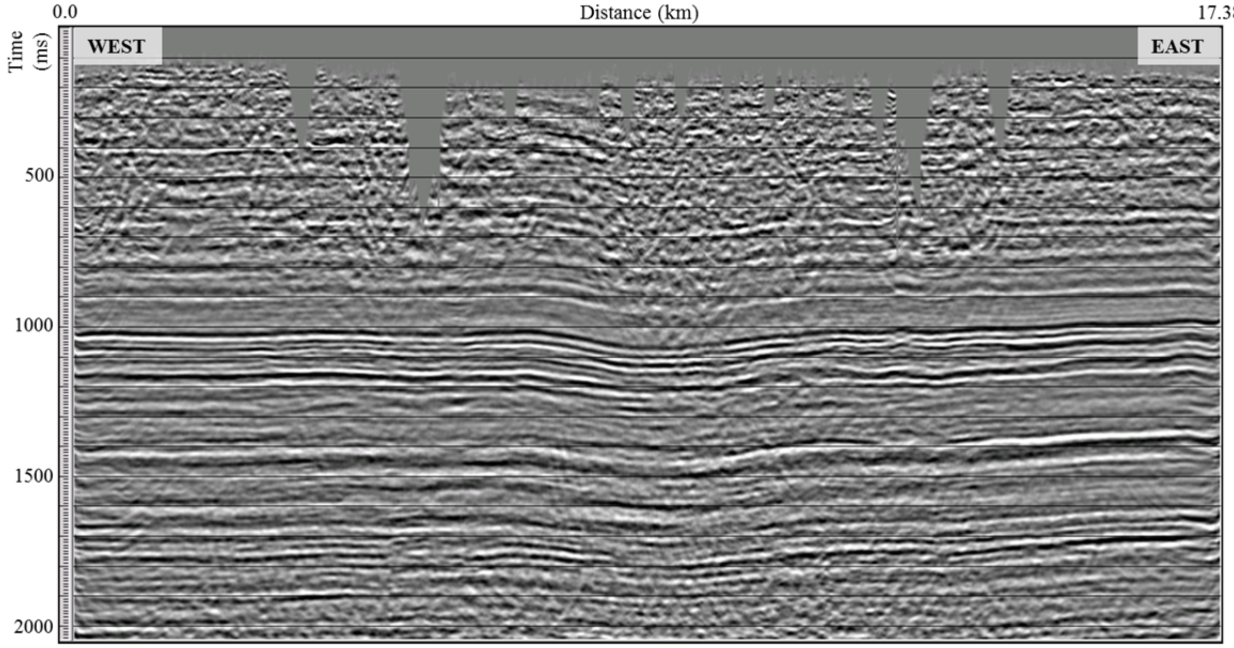

FIG. 3. Highvale stack section new processing.

Figure 4 displays the complete set of logs from Well 8-17.

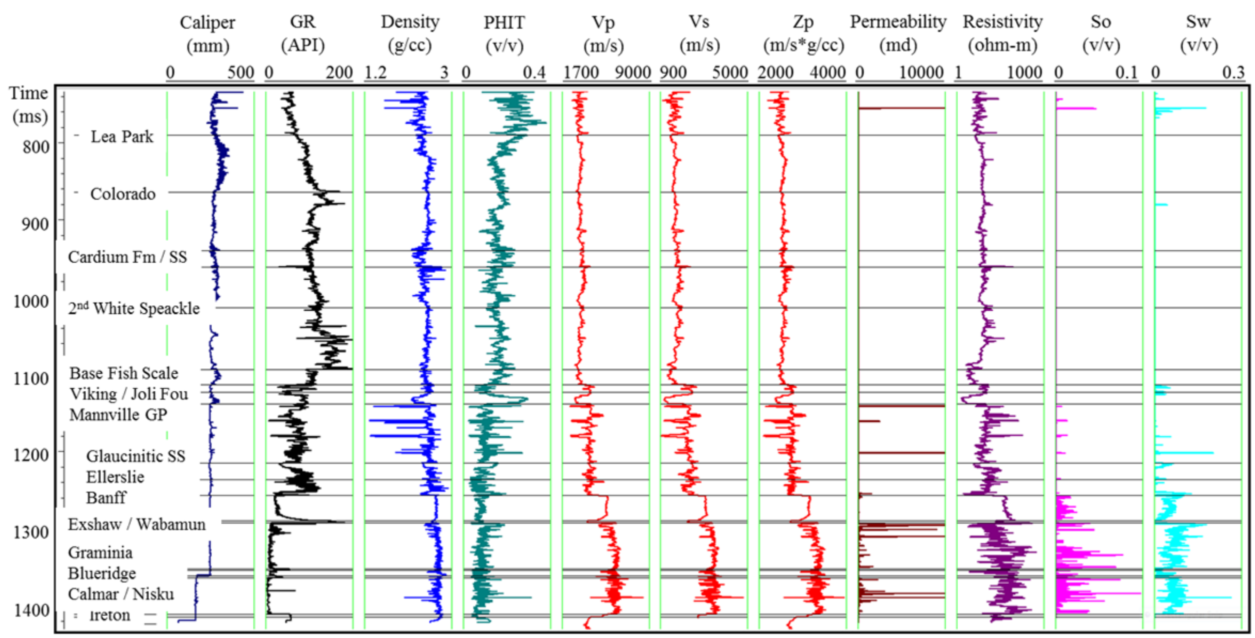

FIG. 4. Well 8-17 with its complete logs suite recorded through the target formation down to a depth of 1900 m.

Processing Overview

The conventional sequence, processed by C&C System, used surface wave noise attenuation and spiking deconvolution processes, while the specialized sequence used radial filter and gabor deconvolution processes. The specialized processing flow resulted in better attenuation of low-frequency noise while succeeded in retaining the low frequency signal. In comparison with the previous processed stacked (Figure 2), new result showed higher low-frequency content around the target zone (~ 5-9 Hz) than the previous processing (~ 9-14 Hz) (Figure 3); but showed a structural depression in the middle part of the section possibly related with a shallow channel caused by an old meander of the North Saskatchewan River. However, no velocity or statics anomalies were observed during the processing of this dataset (Gavotti and Lawton, 2013).

Well log analysis

The well log information for this study was provided by Schlumberger as mentioned previously. Schlumberger undertook a detailed study with this well including core analysis to analyze the capability of the Nisku Formation to store CO_2 as well as testing the Calmar Formation as a seal to avoid potential leakage of the injected gas. Figure 5 shows an image of the core samples from the Nisku and Calmar formations (http://www.cmc-nce.ca/events/gallery/).

FIG. 5. Nisku core sample and Calmar core plug recovered from Well 8-17 during the development of Project Pioneer. Diameter = 1 inch (modified from Carbon Management Canada, 2013: **http://www.cmc-nce.ca/events/gallery/**).

Table 1 summarizes the main properties of the Nisku Formation from analyzing Well 8-17 as well as three others in the Wabamun area (Alshuhail, 2011).

Table 1: Physical properties of the Nisku Formation in the Wabamun Area. The values with an asterisk (*) were obtained from the Well 8-17.

Target Aquifer / Formation	Nisku
Primary Lithology	Dolostone
Reservoir Bearing Fluid	Water (brine)
Other Reservoir Fluid	Gas
Reservoir Depth	1793* m
Reservoir Thickness	103* m
Reservoir Pressure	15 MP
Reservoir Temperature	50.3 C°
CO_2 Phase at the Reservoir	Supercritical
Gas-Water Ratio	4 (insignificant)
Average Effective Porosity	7.4* %
Average Permeability	315* md
Density of Supercritical CO_2	653 kg/m^3

From Table 1 it can be observed that the average effective porosity value of the Nisku Formation is 7.4% and the average permeability is 315 md. In comparison, the average effective porosity of the Calmar Formation is 1.8% and the average permeability is 0.83 md (Alshuhail, 2011). Importantly the differences in these properties are key for reducing the risk of potential leakage.

From the cross plot analysis performed on Well 8-17 it should be possible to differentiate the Nisku Formation from the overlain formations. Since the Calmar Formation has a thickness of 6 m in this area, it is expected that resolving this formation from Graminia and Blueridge formations will be a challenge. The vertical resolution for this dataset is approximated 50 m. Figure 6 shows a cross plot between P-impedance (Zp) and porosity (ϕ) with Gamma Ray (GR) in the colour key. The cross plot was done between tops Banff and Ireton (1256 ms to 1411 ms). Note how cleaner lithologies (GR $<$ 10) separates from more shaly lithologies with high values of P-impedance (Zp $>$ $\sim 16 \times 10^6$ m/s*kg/m^3). The two yellow bars above the Nisku Formation correspond to the Calmar and Graminia formations. In terms of performing an inversion study it would be challenging to resolve these formations.

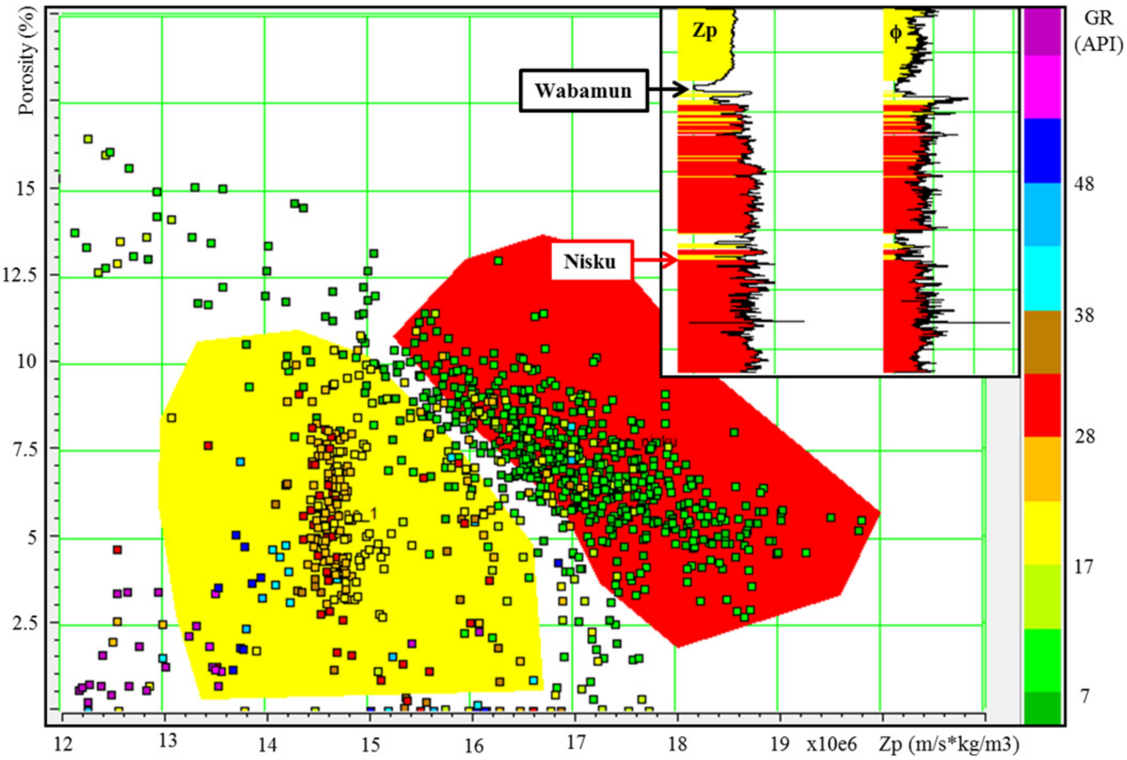

FIG. 6. Cross plot between Zp and porosity and GR in the colour key. Note how Cleaner lithologies (GR < 10) separates from more shaly lithologies with high values of P-impedance (Zp > ~$16x10^6$ m/s*kg/m^3). The two yellow bars above the Nisku Formation correspond to Calmar and Graminia formations.

Seismic-well ties

The seismic-well tie process is based in the correlation of a synthetic seismogram with the seismic data to best match the target log with the seismic attributes that will help in the interpretation of the horizons of interest. The process consists of applying a manual check shot correction by applying bulk shifts and/or stretch and squeeze to the log and modifying the depth-to-time curve to match the P-wave seismic times.

The first step was to extract a constant phase statistical wavelet from the seismic data to start the correlation at each well. The next step was to extract a wavelet for each case and refine the correlation. The algorithm uses both the available wells and the seismic data near those wells. It extracts the wavelet by finding the operator which, when convolved with the reflectivity from the well, closely approximates the proximal seismic traces (Hampson-Russell Software, 2013).

In the first case (a) the wavelet was extracted from the Well 8-17 in a window from 800 ms to 1500 ms (Figure 7) with a final correlation coefficient of 0.738 (Figure 8).

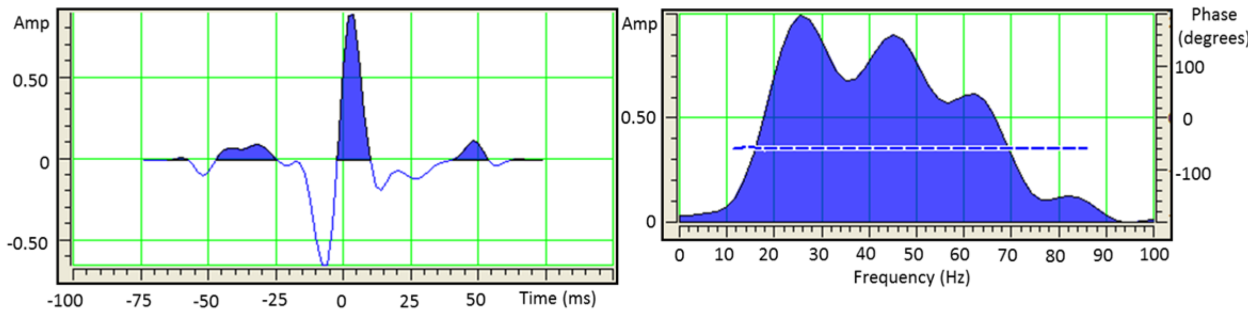

FIG. 7. Wavelet extracted from Well 8-17 in case a) with its amplitude spectrum. The dotted line indicates the average phase of the wavelet (-56°).

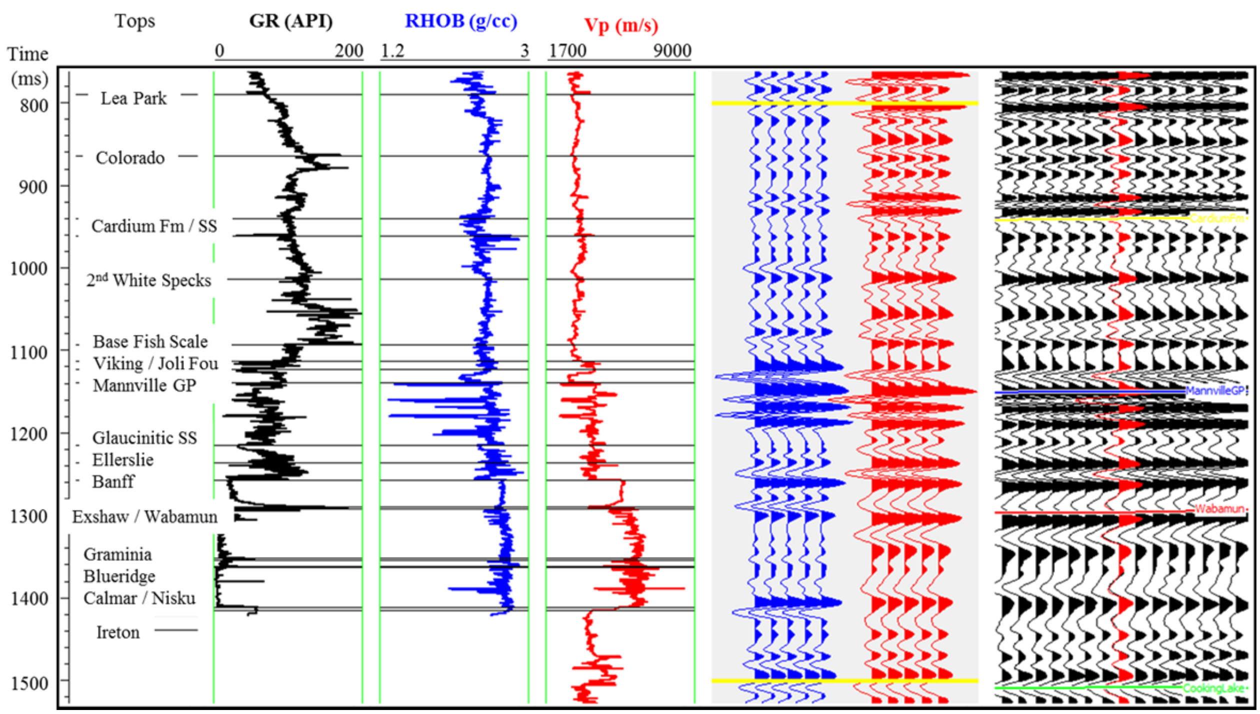

FIG. 8. Final tie of Well 8-17 with the C&C dataset (case a). Blue traces represent the synthetic seismogram; red traces represent the extracted trace from the seismic data at the well location, and black traces shows the ten traces around the well location. Yellow bars show the correlation window. Correlation = 74%.

Figures 9 and 10 show the wavelet and seismic-well tie process for case b). The correlation coefficient was 0.623.

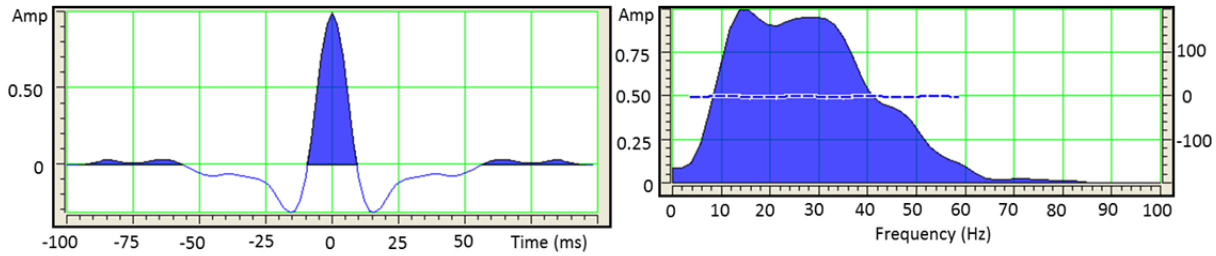

FIG. 9. Wavelet extracted from Well 8-17 in case b) with its amplitude spectrum. The dotted line indicates the average phase of the wavelet (-7°).

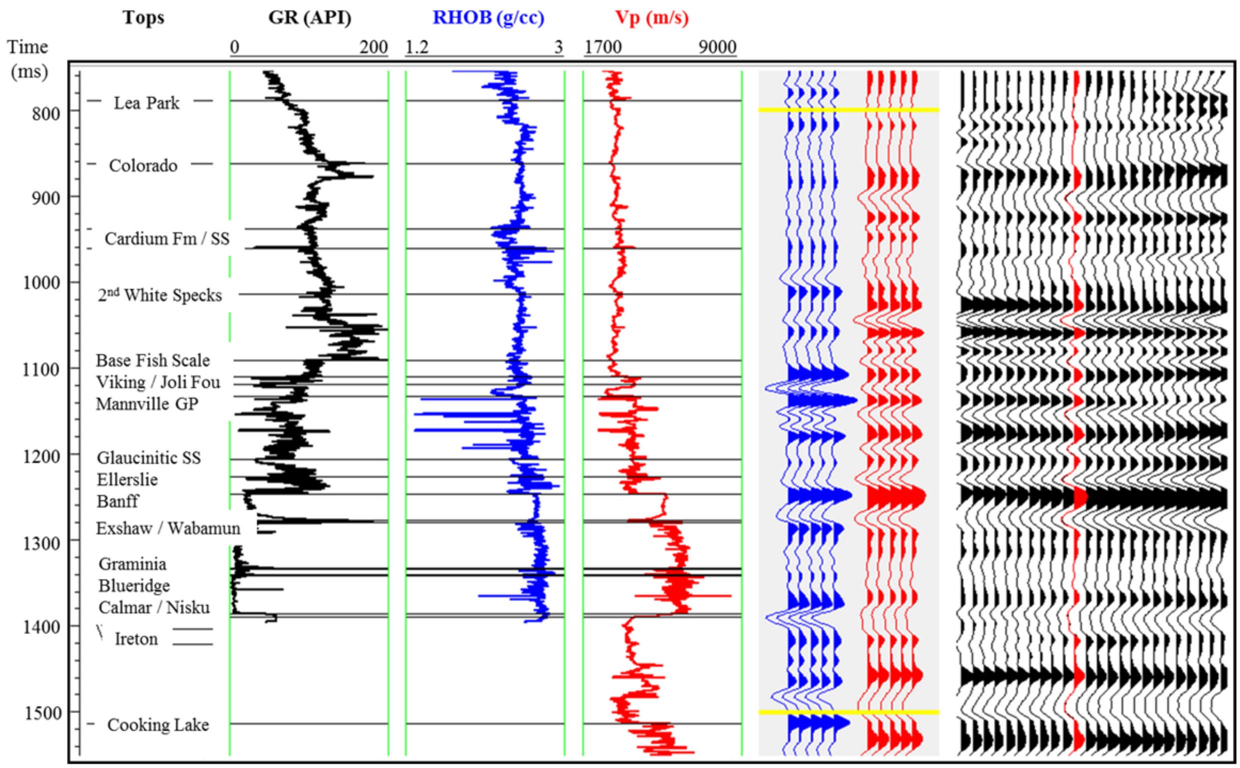

FIG. 10. Final tie of Well 8-17 with the case b) dataset. Blue traces represent the synthetic seismogram; red traces represent the extracted trace from the seismic data at the well location, and black traces shows the ten traces around the well location. Yellow bars show the correlation window. Correlation = 62%.

MODEL-BASED INVERSION

Model for Inversion

The initial background model was formed by blocking an impedance log from a well. The final result is dependent on the initial model so the model must be low-pass filtered to reduce this effect (Lindseth, 1979). The P-impedance (Zp) initial model was generated using a P-impedance log calculated with the sonic and density logs from Well 8-17. In case a), a low-pass filter with a low frequency ramp of 8-13 Hz was applied to build the model (Figure 11); while in case b), the low frequency ramp was 6-10 Hz (Figure 12). P-impedances in the model range from 3.8 to almost 19 m/s*kg/m^3. The 2D impedance model was generated by interpolating the impedance at the well location using the Second White Speckled Shale horizon as a guide in both cases.

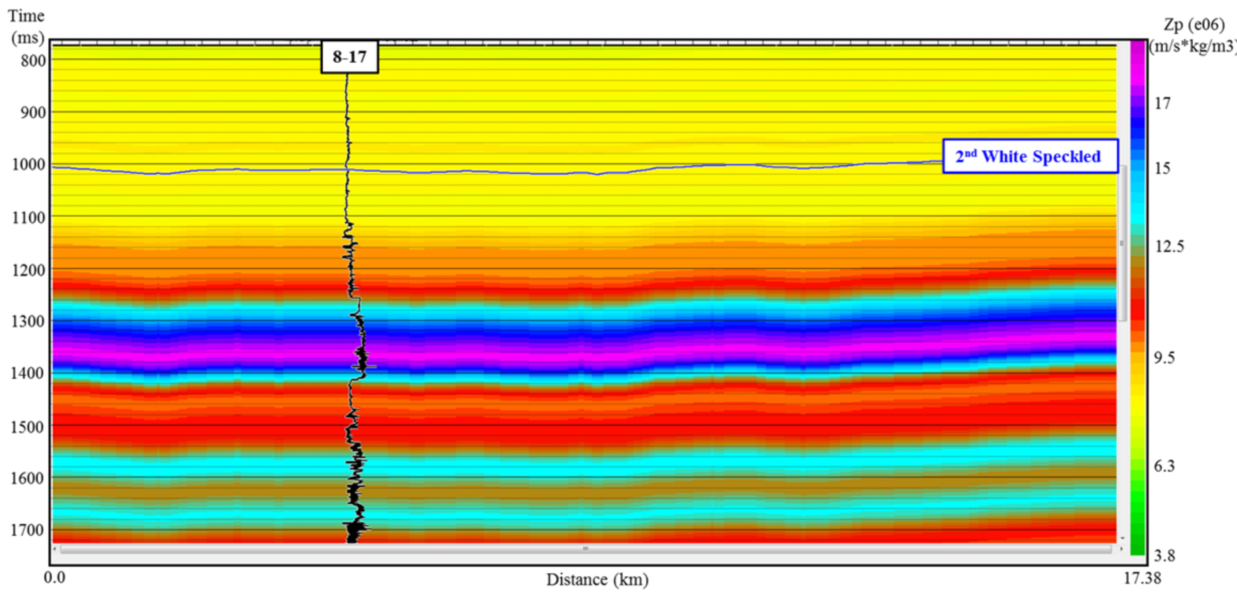

FIG. 11. Initial low frequency P-impedance model (8-13 Hz) using Well 8-17 and the Second White Speckled Shale horizon. The inserted black curve is the Vp log.

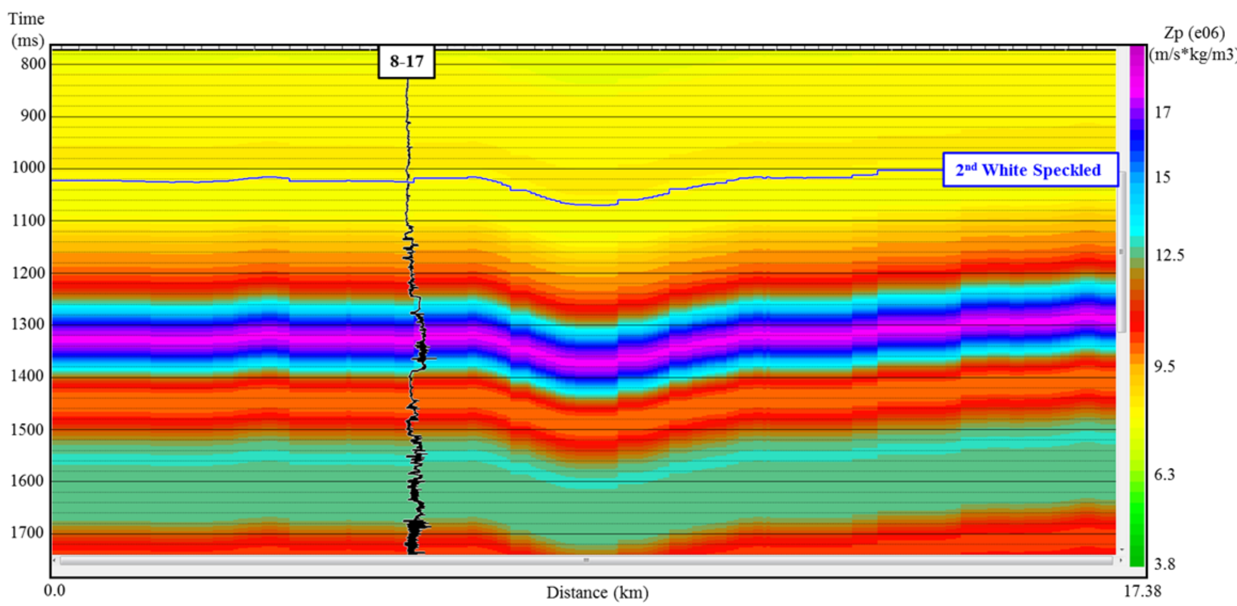

FIG. 12. Initial low frequency P-impedance model (6-10 Hz) using Well 8-17 and the Second White Specked Shale horizon. The inserted black curve is the Vp log.

Inversion Analysis

A post-stack inversion analysis was performed initially at the location of Well 8-17 focused on a window from 800 to 1500 ms, to evaluate the efficacy of the inversion by comparing the impedance at the well with the impedance derived from the seismic data.

The impedance was inverted from a single trace at the well location and was then convolved with a wavelet to produce a synthetic trace that was compared with the actual seismic trace at that location. The correlation between the synthetic trace (red) and the seismic trace (black) is very good in both cases ((a) and (b)) with high correlations coefficients (over 0.99 for case (a) and over 0.96 for case (b)), (Figures 13 and 14 respectively). The estimated RMS error between them is 0.09 and 0.26. The inversion result is band-limited and fails to reproduce the higher frequency details in the impedance observed in the well logs. To make a fair comparison, well logs were filtered using a high-cut of 60/100 Hz. Within the inverted window the inversion estimates are very close to the actual impedance values; however, in the Wabamun Group the inverted impedance shows the general trend and relative variations indicating higher impedance consistent with its lithology. The RMS error between the target log and the predicted log curves is $1.4x10^6$ m/s*kg/m^3.

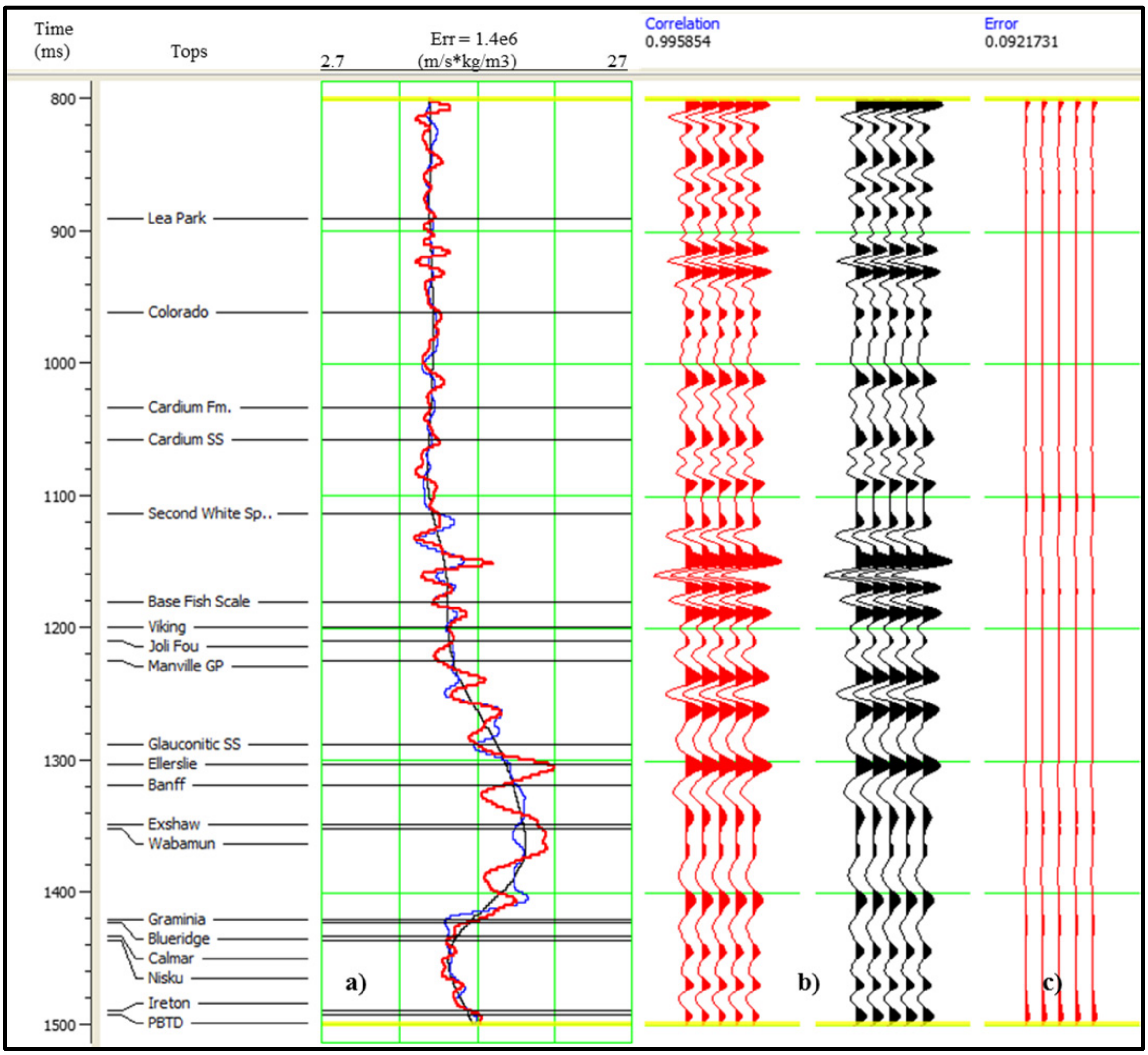

FIG. 13. Analysis of the post-stack inversion at Well 8-17 with the initial model cut-off of 8-13 Hz: a) filtered impedance log (blue), initial model (black), inversion result (red); b) synthetic trace from inversion (red) and extracted trace from the seismic (black), and c) RMS error between synthetic trace and seismic trace.

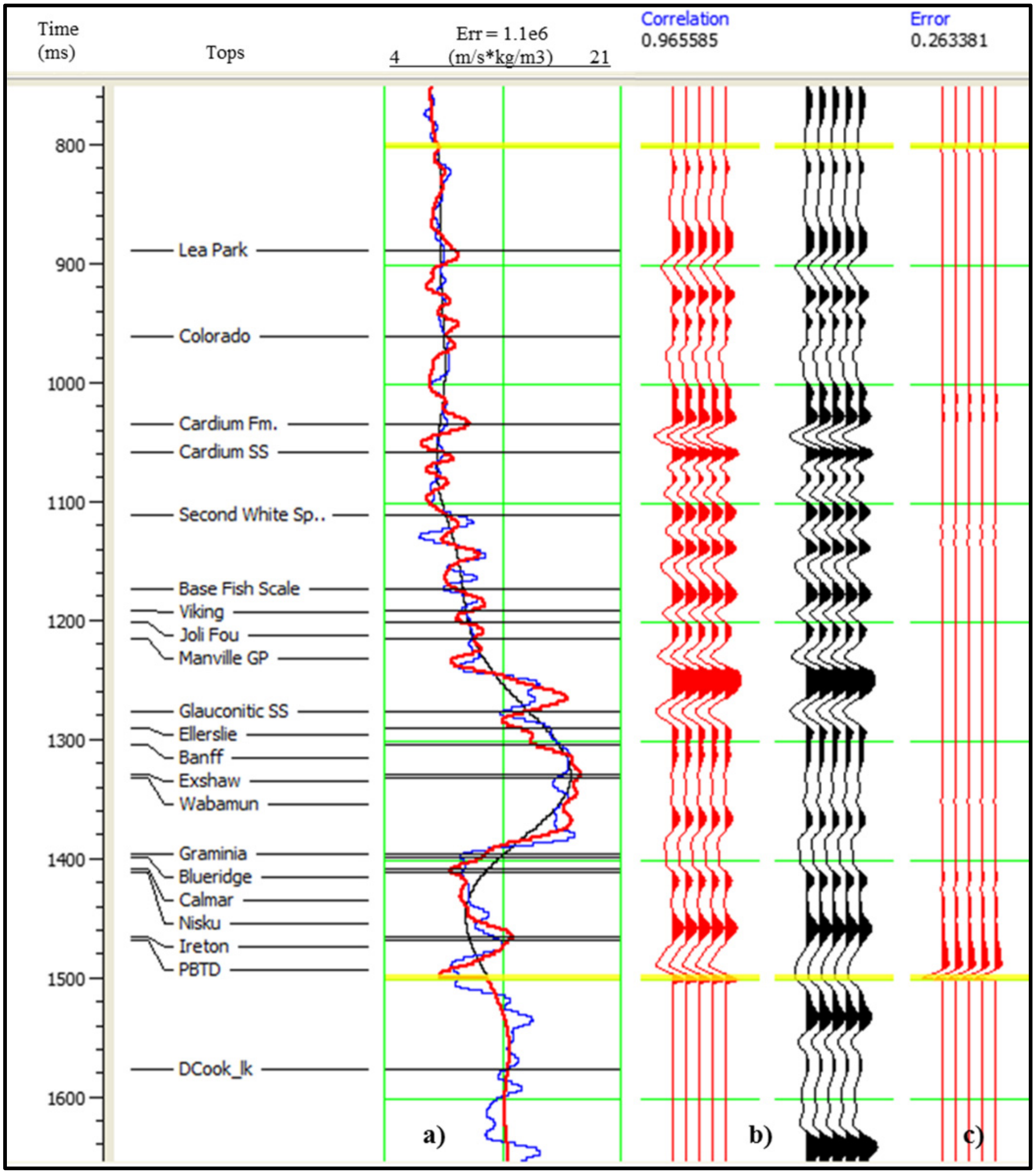

FIG. 14. Analysis of the post-stack inversion at Well 8-17 with the initial model cut-off of 6-10 Hz: a) filtered impedance log (blue), initial model (black), inversion result (red); b) synthetic trace from inversion (red) and extracted trace from the seismic (black), and c) RMS error between synthetic trace and seismic trace.

Inversion Results

Following the analysis at the well location, the model-based inversion of the seismic data was undertaken for both cases. The inversion results of the dataset processed by C&C (case a) (Figure 15) and the newly processed dataset (case b) (Figure 16) show that the inverted impedance is very close to the actual impedance values. In both cases, in the Winterburn Group the Graminia, Blueridge and Calmar formations were not individually resolved as expected because their thicknesses are below the seismic vertical resolution; in which case, the amplitudes of the recorded seismic data are affected by interference effects from surrounding layer boundaries. The inverted impedance of these units merges with that from Wabamun Group with a higher impedance layer in comparison with the underlying Nisku Formation. The Nisku Formation shows impedance values lower than expected ($9x10^6$ – $19x10^6$ $m/s*kg/m^3$) according to the impedance log analysis (> $15x10^6$ $m/s*kg/m^3$, Figure 5); this could be associated with the higher porosity and permeability of this formation in comparison to the overlying formations plus the fluids present in the Nisku formation (water and gas) which affect the impedance response. Underlying the Nisku Formation, the Woodbend Group shows intermediate (~$11x10^6$ $m/s*kg/m^3$) and lower (~$8x10^6$ $m/s*kg/m^3$) impedance values corresponding to the lithologies of these different units, (limestones and shales). The P-impedance log filtered with a high cut of 60/100 Hz was inserted for comparison with the inversion result. Although similar results are seen in both cases, in general case a) shows more continuous layers without much lateral variation. Meanwhile, case b), shows thicker layers with some lateral variations possibly due to the effect of the initial model that has lower frequency content than that used in case a). Also, the case b) result shows higher resolution within the Colorado Group, below Second White Speckled Shale.

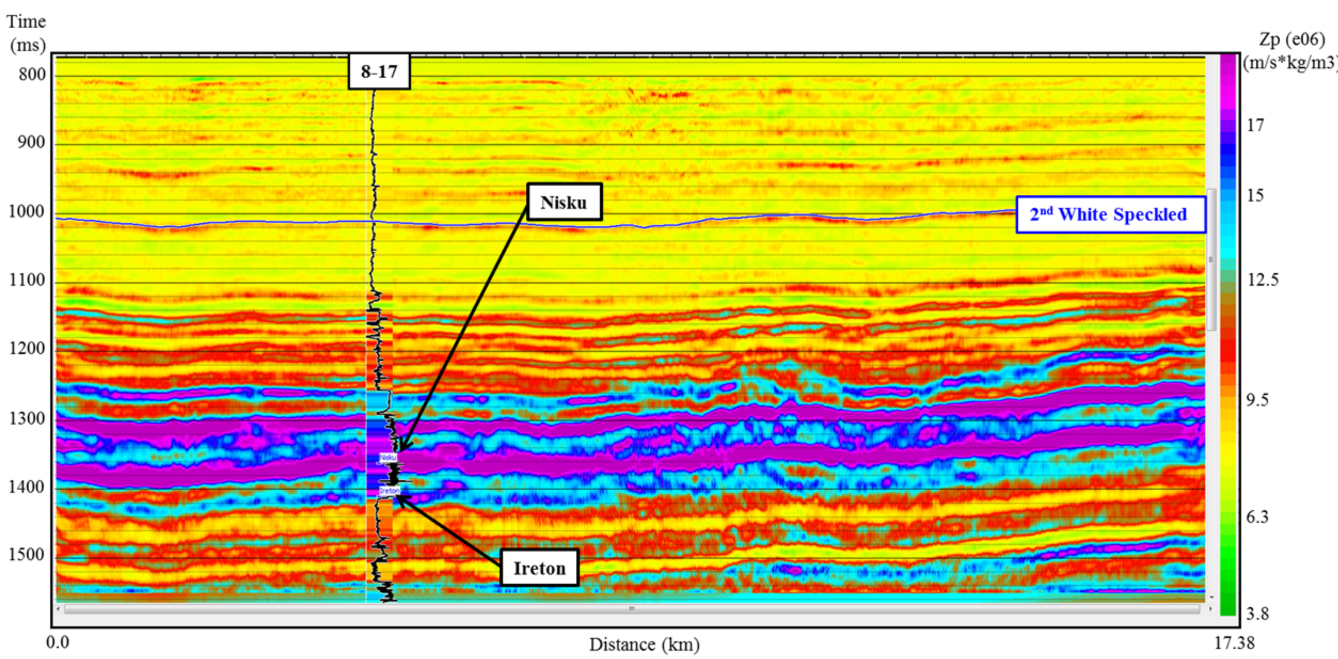

FIG. 15. Inversion result of the Highvale seismic data based on previous processing (case a) showing the gamma ray curve in black and the impedance log with a high-cut filter 60/100 Hz in color at the well location for comparison.

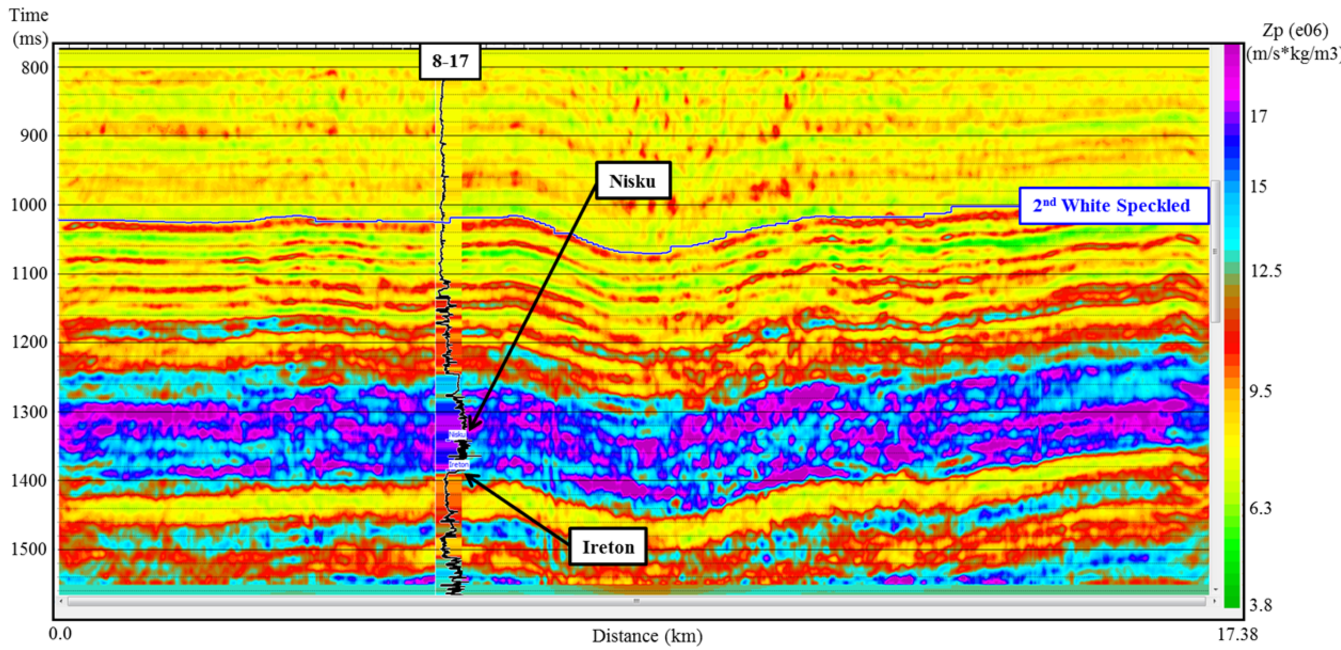

FIG. 16. Inversion result of the Highvale seismic data based on new processing (case b) showing the gamma ray curve in black and the impedance log with a high-cut filter 60/100 Hz in color at the well location for comparison.

Figures 17 and 18 show with more detail the inversion results within the Wabamun and Winterburn Groups. In both cases, the inversion result at the well location is excellent and with high correlation as indicated in the inversion analysis. Despite the depression observed in case b), no major differences are seen in terms of vertical position of the units at the well location and in the relative variation of the inverted impedance values.

Another important difference is that in case b), the initial model presented several high frequency features related to the horizon used to interpolate the model (Figure 12). These features are not observed in the inversion result. Even though the horizon comes from interpreting the seismic data, the inverted impedance is related more to impedance changes at the layer boundaries and the fact that these spikes are not present in the result indicates that the seismic data is dominating the inversion process.

Case a) result presents a cleaner section possibly due to higher apparent resolution evident in the final stack. Case b) result shows more low frequency content from the seismic instead of adding it from the wells in the initial model. This result also proves the importance of taking particular care in the noise attenuation processes during processing to avoid removing low frequency signal which is vital in inversion studies.

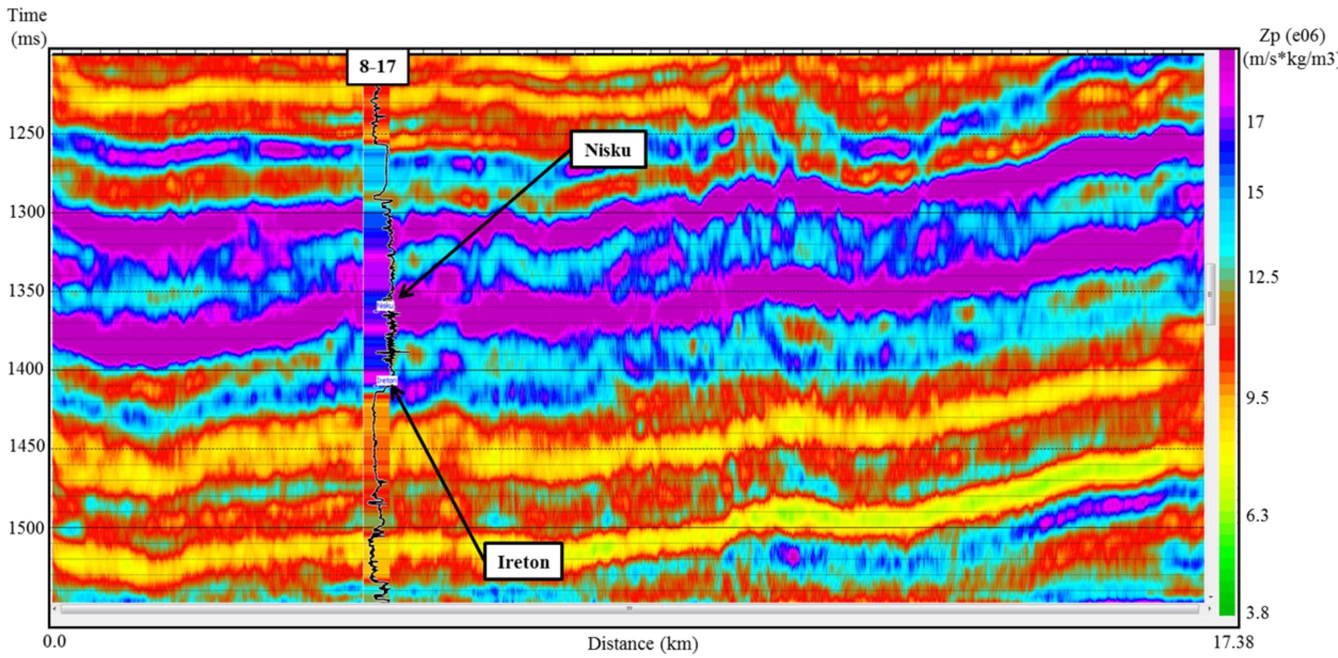

FIG. 17. Inversion result of Highvale line previous processing (case a) on Wabamun and Winterburn Groups with the gamma ray curve in black and the impedance log with a high-cut filter 60/100 Hz inserted in colour at the Well location for comparison.

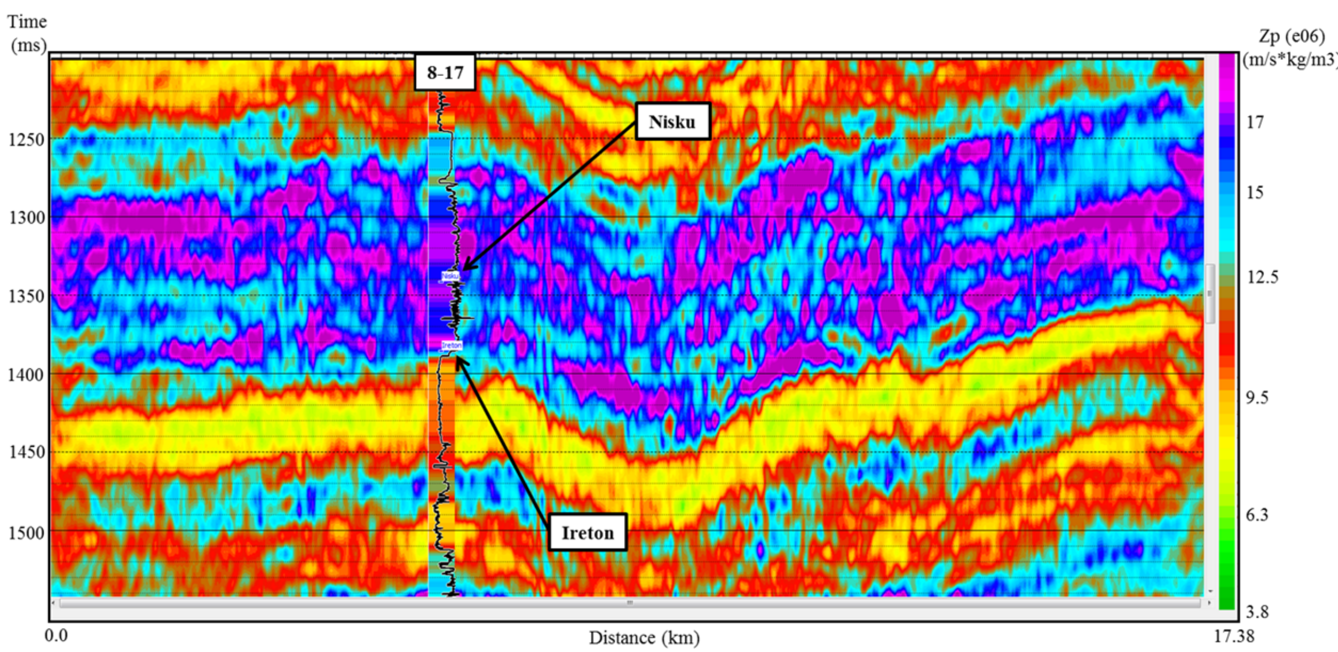

FIG. 18. Inversion result of Highvale line current processing (case b) on Wabamun and Winterburn Groups with the gamma ray curve in black and the impedance log with a high-cut filter 60/100 Hz inserted in colour at the Well location for comparison.

2D SEISMIC MODELLING

2D Geological Modelling

The 2D geological model consisted of a 17.38 km long cross-section, created using Norsar-2D software. The structure of the section was based on the parameters of the Highvale line. The geological model was designed combining geological background and well log information from Well 8-17.

To reproduce the stratigraphy and layering of the model, gamma ray, velocity and density logs were used. Based on the seismic character from data, a flat layer design was chosen to reproduce the local geologic model. The units utilized in defining the blocks were selected based on the key formation tops identified in the logs as well as the seismic data. Fourteen layers were defined based on the average values of the target logs for each of them (Figure 4). Table 2 summarizes the velocities and density values for each block.

Table 2: Geological model parameters. The target formation is indicated in red

Block	Depth (Km)	Vp (m/s)	Vs (m/s)	ρ (g/cc)	Formation
1	0.0	1900	1590	2.3	Shallow surface
2	0.1	1920	1600	2.3	Shallow - Lea Park
3	0.773	3000	1610	2.35	Lea Park
4	1.27	3300	1620	2.5	Viking
5	1.533	3700	2000	2.68	Banff
6	1.605	5410	3029	2.61	Exshaw
7	1.613	3795	2195	2.74	Wabamun
8	1.764	6000	3300	2.67	Graminia
9	1.769	5889	3328	2.78	Blueridge
10	1.787	5890	3350	2.77	Calmar
11	**1.793**	**5500**	**3150**	**2.8**	**Nisku**
12	1.897	6200	3300	2.77	Ireton
13	2.0	5000	2660	2.8	Duvernay/Leduc
14	2.14	4000	2100	2.77	Basal Cooking Lake

The option “Model Builder” from Norsar-2D software was used to create the geological model. This option allows defining the geometry of the model by setting the boundaries in terms of distance and depth (X and Y coordinates). In this rectangular section, a series of interfaces were created to represent the geological structure of the study area. The depth of each interface is also defined in terms of its coordinates. Once these interfaces were created, the space between each of them represents a block. These blocks are then filled with the properties Vp, Vs and density obtained from the well log values summarized in Table 2. Figure 19 shows the baseline geological model. The model size is 17.38 km long and 2.5 km deep. The Nisku Formation is the 11th block found at a depth of 1.793 km.

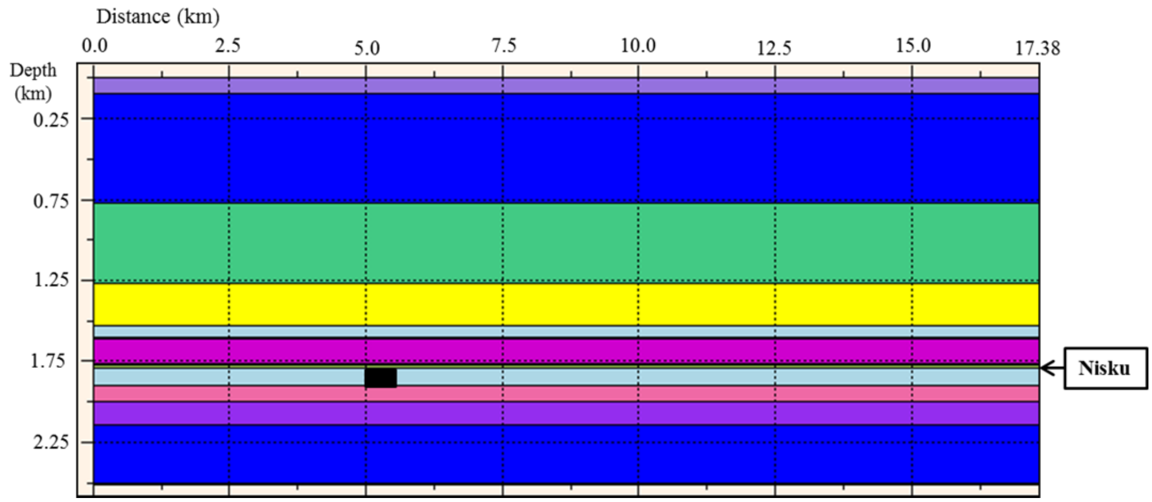

FIG. 19. Geological model. The location of the injection zone in the Nisku Formation is indicated by the black rectangle.

CO_2 Plume Simulation

Frailey (2009) explained the methods for estimating the volume of CO_2 trapped in geological formations. The static approach requires rock and fluid properties while the dynamic approach requires information about active injection, injection volumes and reservoir pressure. The static technique was applied in this project, specifically the volumetric method which is summarized in Figure 20. A cylinder or disk was selected to estimate the CO_2 volume and corresponding radius of extension (Vera, 2012).

The volume of CO_2 is given by the formula:

$$G_{CO2} = Ah\phi E$$

A = area
h = thickness
ϕ = porosity
E = efficiency or saturation

G_{CO2} is also defined by:

$$G_{CO2} = \frac{m}{\rho}$$

m = mass
ρ = density

The geometry of the expansion is represented by a disk with the following area:

$$A = \pi r^2$$

r = radius of the disk of CO_2 expansion

Rearranging the terms, the radius of the CO_2 plume can be obtained from:

$$r = \sqrt{\frac{G_{CO2}}{\pi h \emptyset E}}$$

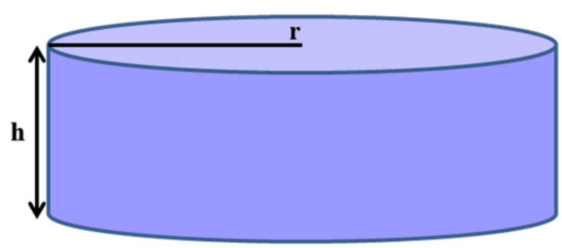

FIG. 20. CO_2 plume designed.

The amount of CO_2 simulated in this experiment was 1 million tonnes after one year of injection. Based on the data presented at Chapter 3, the Nisku Formation has a thickness h = 103.85 m, porosity ϕ = 7.3% and density ρ = 653 kg/cc. The efficiency, considered as the CO_2 saturation, was estimated for 100% saturation (E = 1) in the available pore space. Using the equations in Figure 20 the radius of the disk was calculated to have a value of 253.57 m.

It is important to notice that even when a 3D model was used to estimate the plume size the final geological model is in 2D, therefore the presented cylinder was translated into a rectangle with a longitude equal to the diameter of the cylinder (d = 507.14 m).

The monitor geological model represents the post-injection scenario. For this case, the rectangular CO_2 plume was inserted in the same geological model of the baseline case. Two new interfaces had to be defined to introduce this plume (Figure 21). The layer corresponding to the Nisku Formation was divided in three parts where two of these intervals have the same properties as the baseline model (representing 0% of CO_2 saturation). The third interval represents the injection zone, with velocities and density change values obtained from the Gassmann fluid substitution analysis done by Ashuhail (2011), summarized in Table 3.

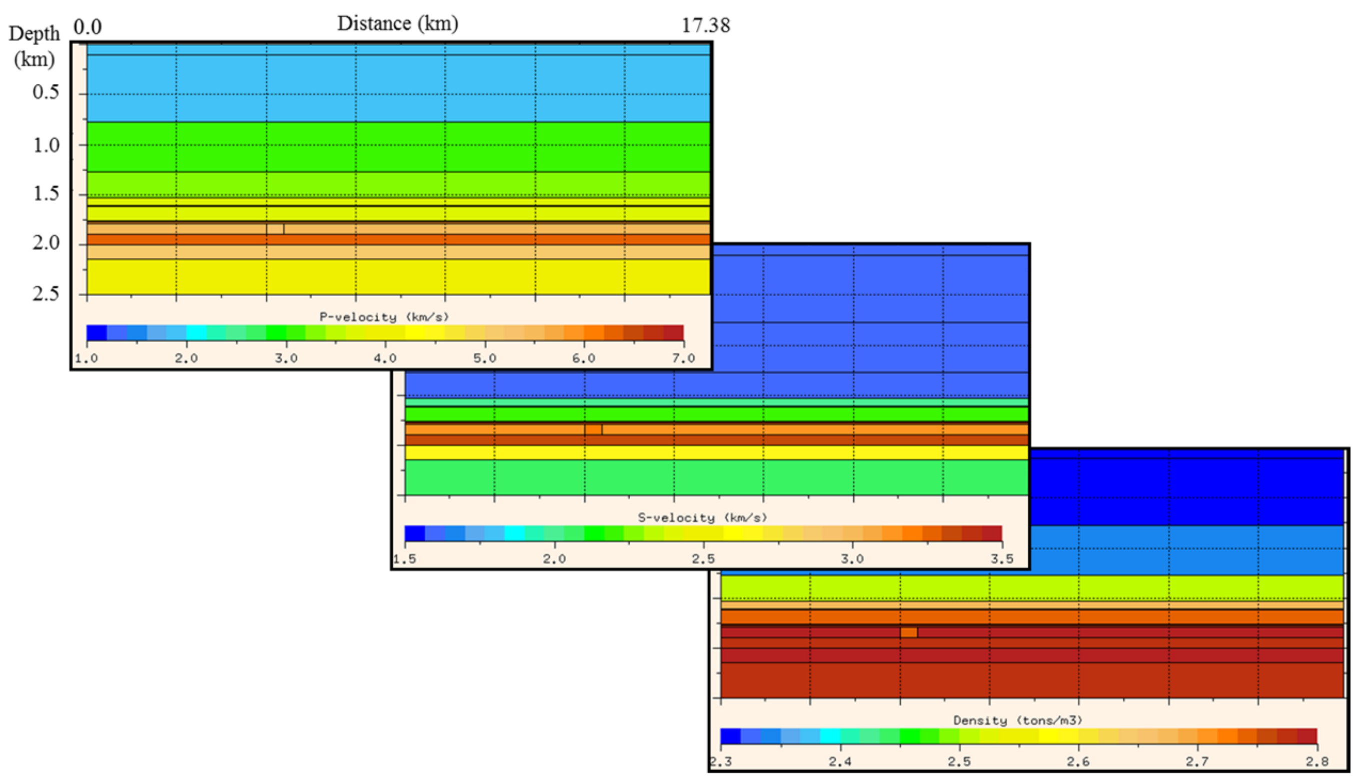

FIG. 21. Monitor 2D geological model (Vp, Vs and ρ). The rectangular CO_2 plume is inserted in the Nisku Formation.

Table 3: Velocities and density values of the CO_2 plume. The percentages change was obtained from the Gassmann fluid substitution analysis performed by Alsuhail (2011).

Properties	Percentage change (%)	Initial values	New values
Vp (m/s)	-4.5	5500	5252.5
Vs (m/s)	0.635	3150	3170
P (g/cc)	-1.26	2.8	2.76

2D Seismic Modelling

The 2D geological models generated previously were input into the 2D seismic modelling algorithm. The goal was to generate the seismic data that would allow performing the time-lapse analysis for monitoring the CO_2 plume. The seismic survey was designed using the same acquisition parameters of the Highvale line and these are shown in Figure 22. The line length is 17.38 km, shots spacing is 80 m, receiver spacing is 20 m. The total number of channels is 200 and the array is split-spread with an offset maximum of 2000 m. NORSAR-2D "Common Shot Ray Tracer" algorithm was used to obtain the reflectivity events which were later convolved with a zero-phase Ricker wavelet of 30 Hz to create the synthetics seismograms for each case. Figure 23 shows an example of a shot gather from the baseline case where the reflections represent the 17 interfaces.

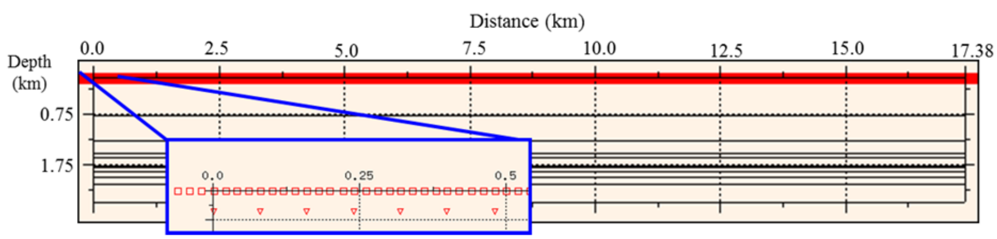

FIG. 22. 2D seismic modelling survey design. The line is 17.38 km long with 80 m shots spacing and 20 m receivers spacing.

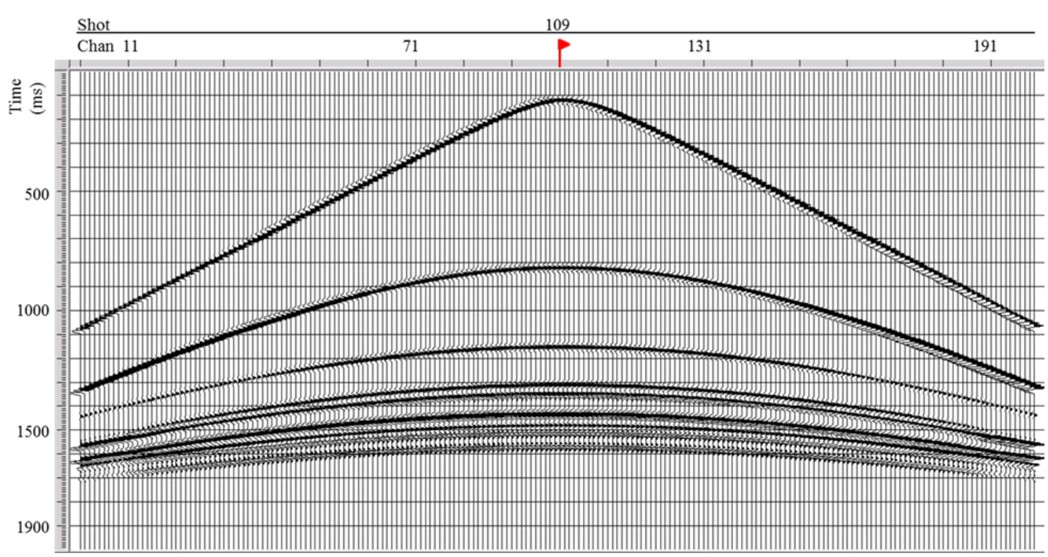

FIG. 23. Shot gather 109 from baseline 2D modelling. 200 channels per shot.

Since no noise or statics effect are present in these models the steps to stack the shot gathers consist of, after assigning the geometry, applying the NMO correction and creating the CDP stacked section. The NMO correction needs a RMS P-wave velocity function (Figure 24) which was obtained from converting, through Dix's equation (Dix, 1955), the interval velocity field defined in the geological models (Tables 2 and 3).

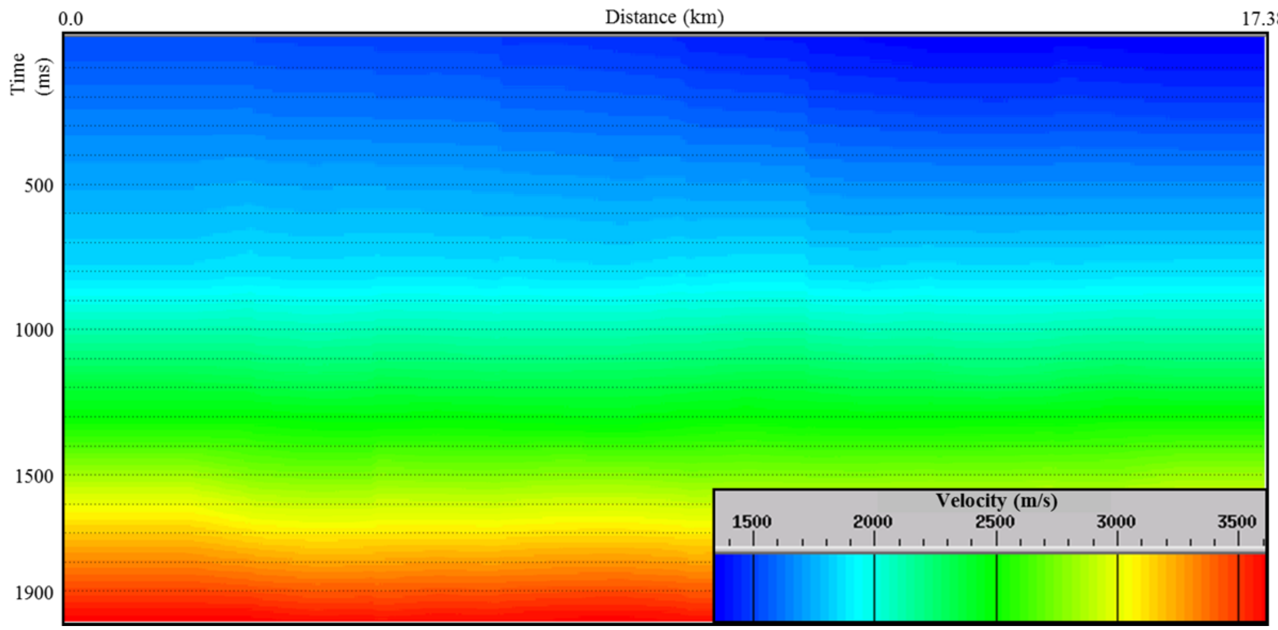

FIG. 24. RMS P-wave velocity field converted from the interval velocity field defined in the 2D baseline geological model.

Figure 25 shows the result of the NMO correction and the stacking processes where a) it is the CDP stack section of the baseline case (0% CO_2 saturation), while b) it is the CDP stack section of the monitor case (100% CO_2 saturation). In the monitor section the injection zone in the target formation is evident. A time shift in the base of the plume and amplitude distortion below it is clearly observable.

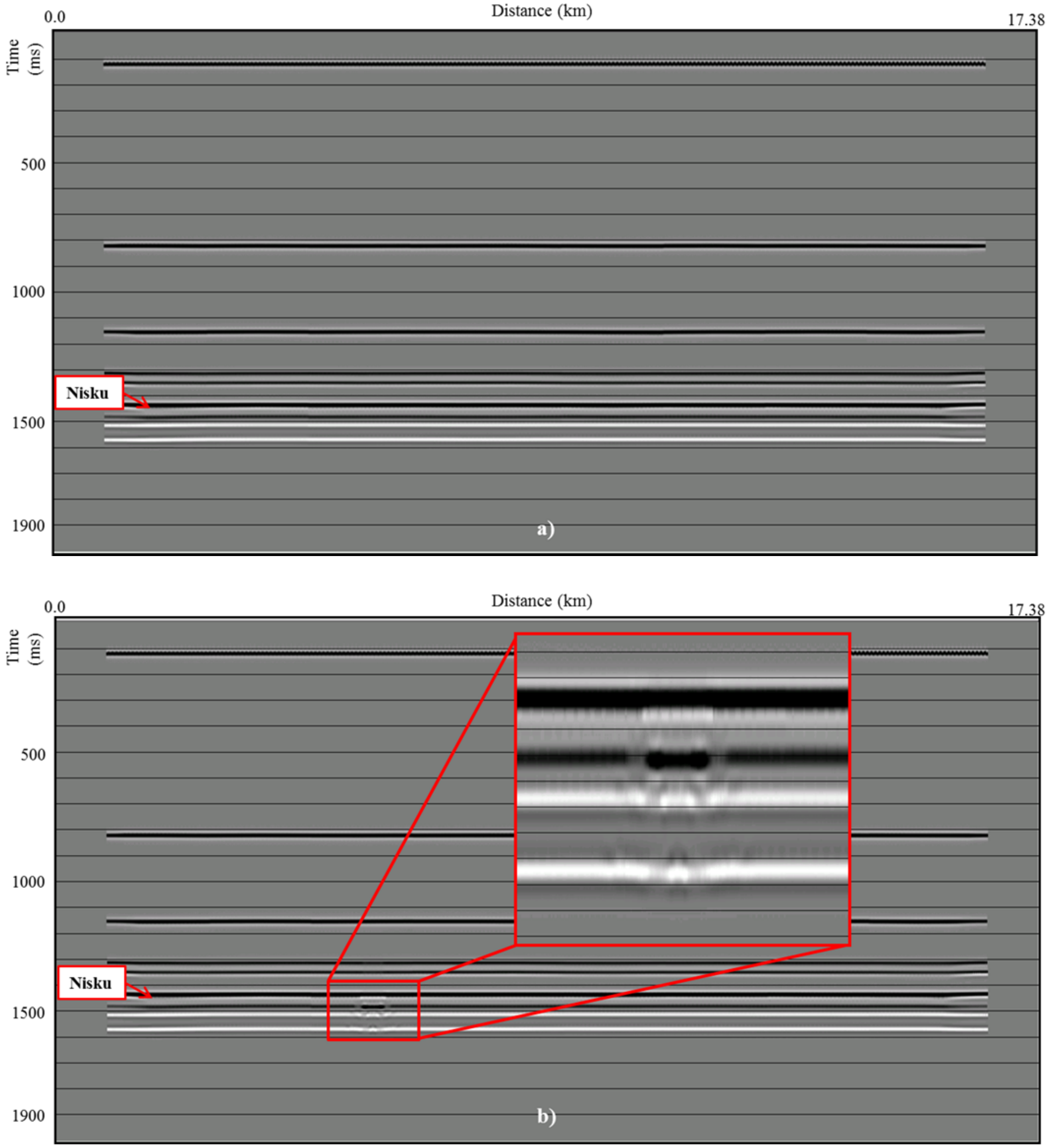

FIG. 25. a) Baseline CDP stacked section, b) Monitor CDP stacked section. Injection zone is indicated in red square.

2D Seismic Monitoring Results

Seismic methods in monitoring CO_2 sequestration programs attempts to identify the CO_2 plume in seismic images by comparing the seismic data acquired before and after injection. From the difference in this time-lapse study it is expected a series of sub-horizontal high amplitude reflections with an underlying velocity pushdown (Chadwick et al., 2006). The main goal of monitoring CO_2 storage is demonstrate the safe storage of the CO_2 in the selected geological site, image the location of the CO_2 plume, and early detection of any leakage.

Since Vp, Vs and density change after injecting CO_2, the effect on acoustic and shear impedances should also change as CO_2 saturation increases, especially if it is different from the surrounding stratigraphy (Sparlin, 2010). The acoustic impedance effect results in an amplitude change that is stronger in magnitude and, therefore, should be more discernible and reliable than P-wave seismic data.

Once the 2D seismic modelling was completed, the next step was to analyze the changes in physical properties, such as reflectivity, time shift and velocity in the monitor data.

Seismic Amplitudes Direct Comparison:

Figure 26 shows the effect in the injection zone determined from subtracting the monitor CDP stacked section data from the baseline section data. This difference represents 100% CO_2 saturation in the injection zone. The traces outside the injection area were cancelled and only the injected region and reflectors below it are affected. This response is made up of the difference in amplitude and travel time expected from the changes that fluid substitution produces in the seismic data.

FIG. 26. Difference between baseline CDP stack and monitor stack. The red square highlights 100% CO_2 injection zone.

In order to quantify these changes, traces at CDP location 726 were extracted from both the baseline and monitor sections. Figure 27 shows the comparison of these traces. The reflection from the base of the Nisku Formation shows a time shift of 1.81 ms, and the RMS amplitude increased over a window from 1452 ms to 1482 ms by about 30% after injecting CO_2.

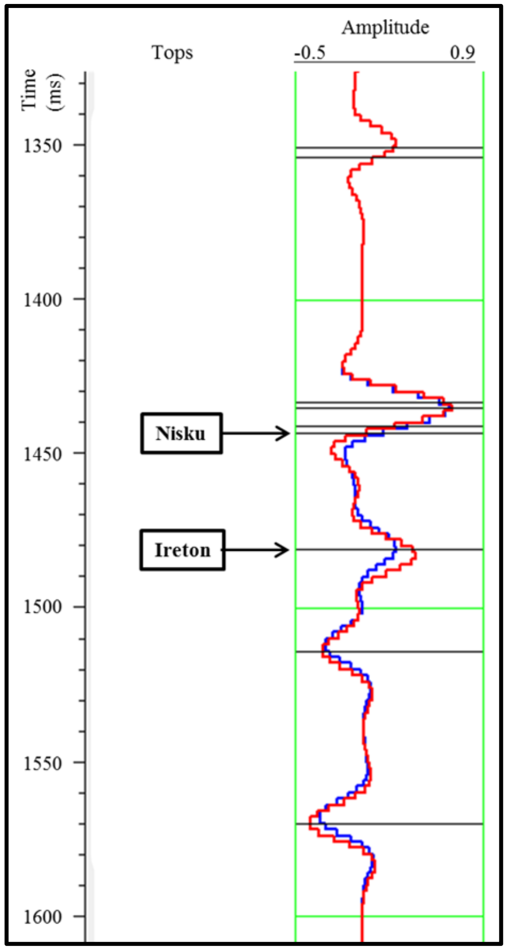

FIG. 27. Comparison of baseline (blue) and monitor (red) traces at CDP location 726.

The edges and top of the CO_2 plume is clearly identified in Figure 26. However, the bottom of the plume is hard to isolate from the reflectors underneath due to velocity pushdown in the monitor survey. The edges of the plume are located between CDPs 702 and 752. Each CDP is separated by 10 m meaning that the width of the plume has a value of 500 m, accurately predicted from the geological model and the difference section.

Impedance Comparison after Seismic Inversion:

A model-based inversion was performed on each CDP stacked section (baseline and monitor) to evaluate the impedance sensitivity in detecting the CO_2 plume.

Since in this case synthetic data is been used, the first step was to create synthetic well logs (Vp and ρ) to help constrain the impedance initial model. The Vp and density values (Table 2) used to build the 2D geological model were used to create these well logs. Figure 28 shows the broadband wavelet from the seismic for the well tie process of the synthetic well logs with the baseline section (Figure 29). The final correlation coefficient was 0.93.

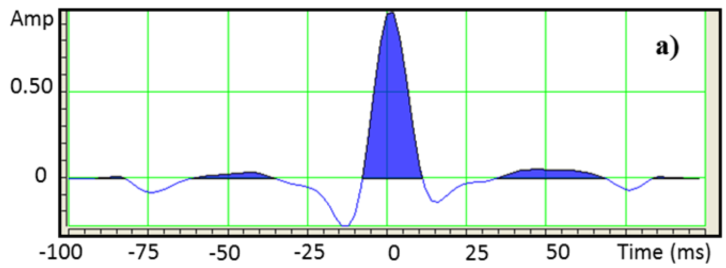

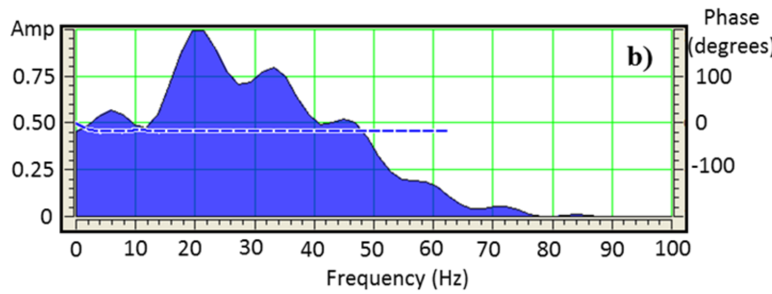

FIG. 28. a) Wavelet extracted from synthetic well with the baseline CDP stack section. b) Amplitude spectrum. The dotted line indicates the average phase of the wavelet (-14°).

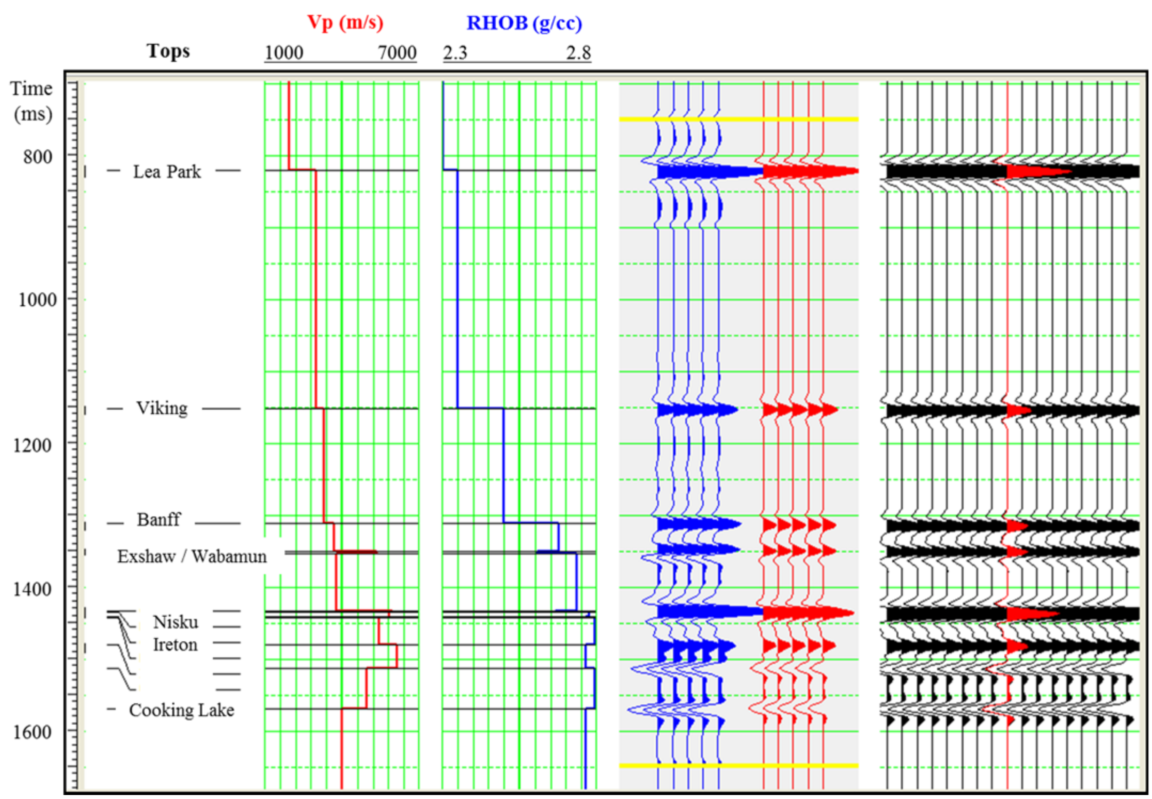

FIG. 29. Tie process of synthetic Vp and density logs with the baseline CDP stacked section. Blue traces represent the synthetic seismogram; red traces represent the extracted trace from the seismic data at the well location, and black traces shows the ten traces around the well location. Yellow bars show the correlation window. Correlation = 93%.

The P-impedance (Zp) initial model was generated using a Zp log calculated with the sonic and density logs from the synthetic well. Since synthetic data is used in this analysis, no low-pass filter was applied in this case. The initial model was generated using the exact impedance values of the synthetic Zp log. P-impedances in the model range from $4x10^6$ to almost $16.5x10^6$ $m/s*kg/m^3$. Figure 30 shows an example of the inversion analysis performed with the initial model and the baseline CDP stacked section in a window from 750 ms to 1650 ms. The correlation between the synthetic (red) and the seismic trace (black) has a high correlation coefficient (0.99). The estimated RMS error between synthetic trace and the seismic trace is 0.053. The RMS error between the target log and the predicted log curves is $3.49x10^5$ $m/s*kg/m^3$.

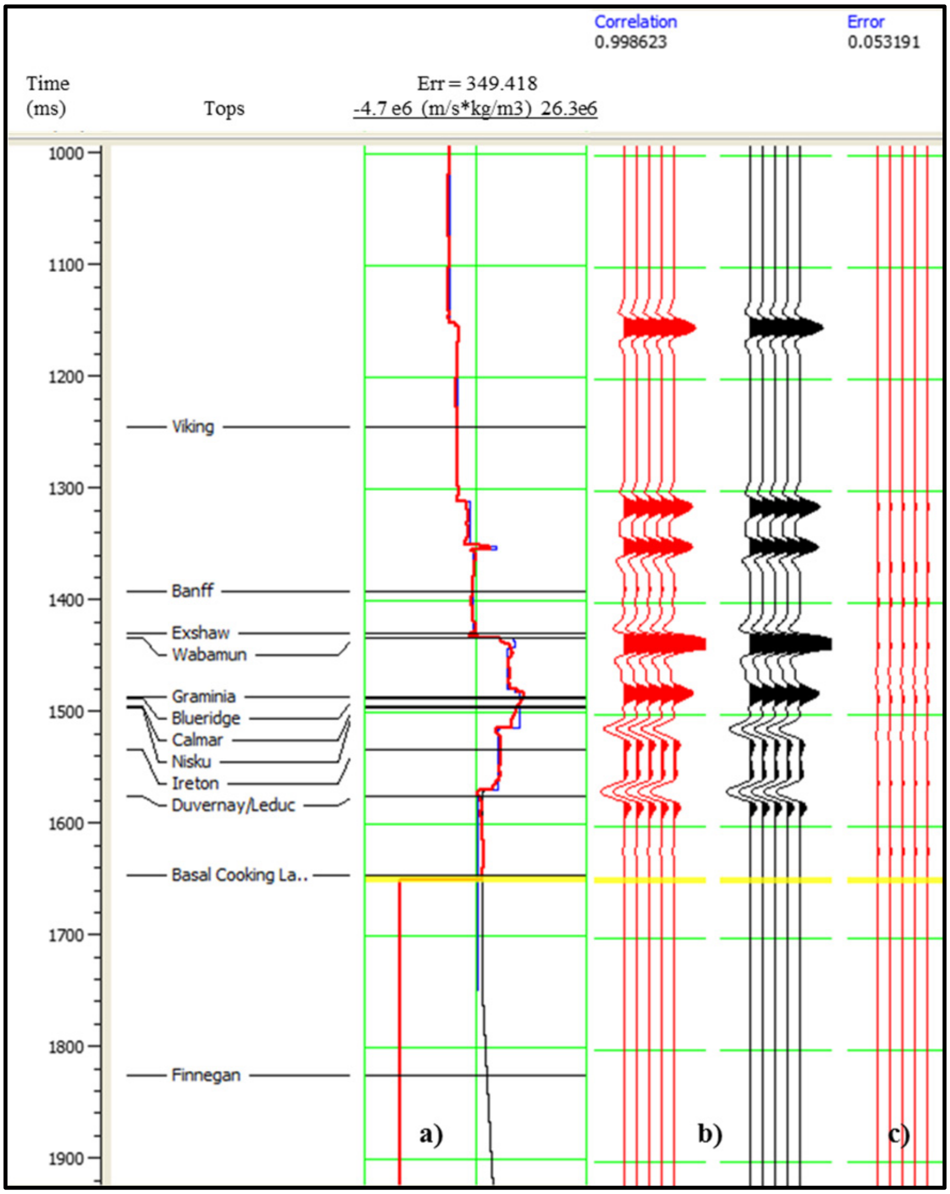

FIG. 30. Analysis of the post-stack inversion at synthetic well location: a) filtered impedance log (blue), initial model (black), inversion result (red); b) synthetic trace from inversion (red) and extracted trace from the seismic (black), and c) RMS error between synthetic trace and seismic trace.

Following the analysis at the well location, the model-based inversion was undertaken for the baseline and monitor datasets. Figure 31 shows the inversion results of (a) the baseline CDP stacked section and (b) the inversion results of the monitor CDP stacked section. The inverted impedance shows the exact impedance values of the initial model except in the monitor case where a distortion is evident in the injection zone and the impedance values of the plume have decreased.

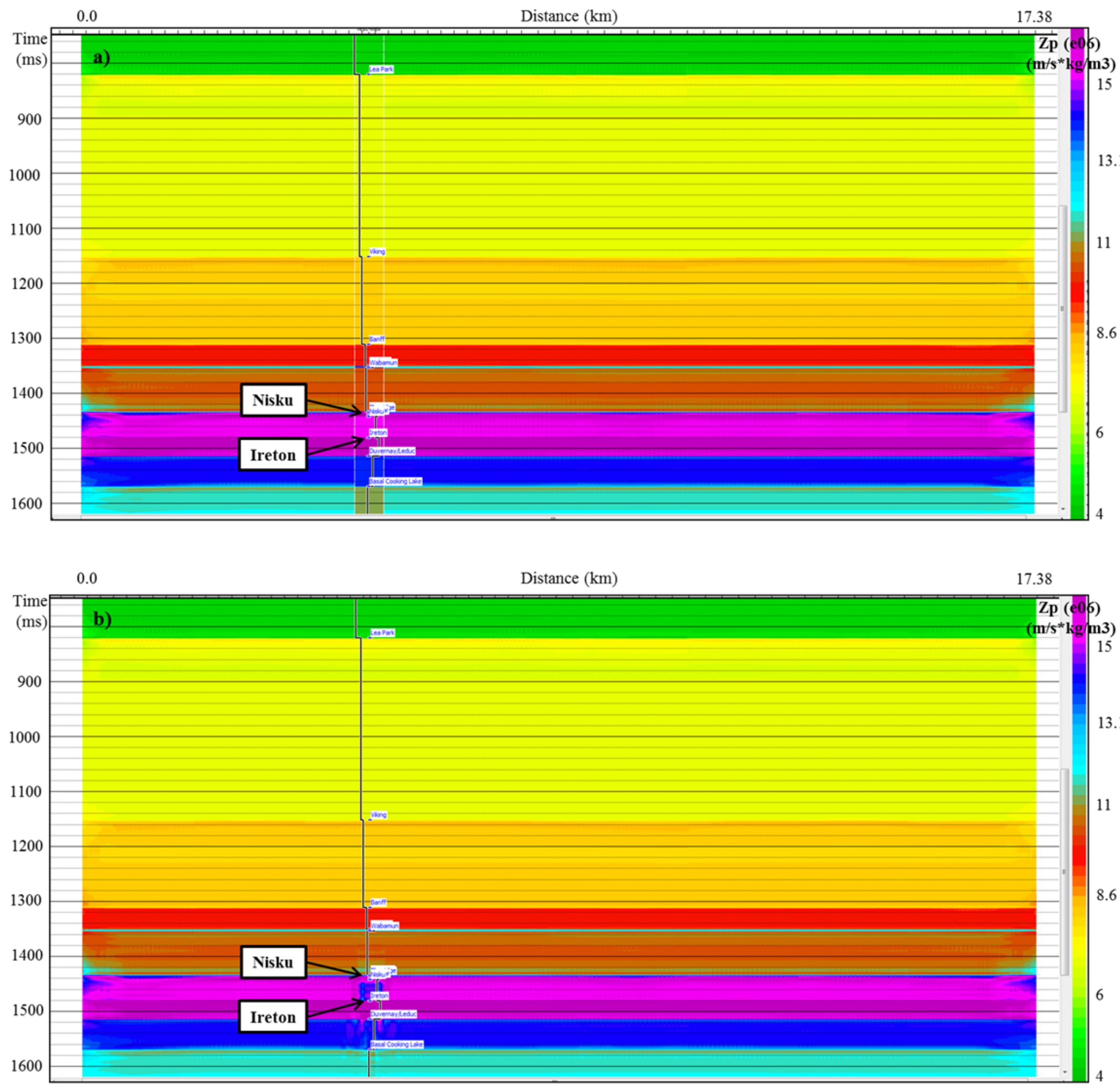

FIG. 31. a) Baseline inversion, b) Monitor inversion. Distortion in the impedance values in the injection region and reflectors underneath is evident.

Numerical impedance changes in traces at CDP location 726 were extracted from the inverted baseline and monitor sections. Figure 32 shows the comparison of these traces. A decreased in the impedance values of ~7% is observed after injecting CO_2 in the Nisku Formation. This percentage enhances the detectability of the plume since combining the effect of Vp and ρ, is effective and is in agreement with the expected values from the fluid substitution analysis (Table 3).

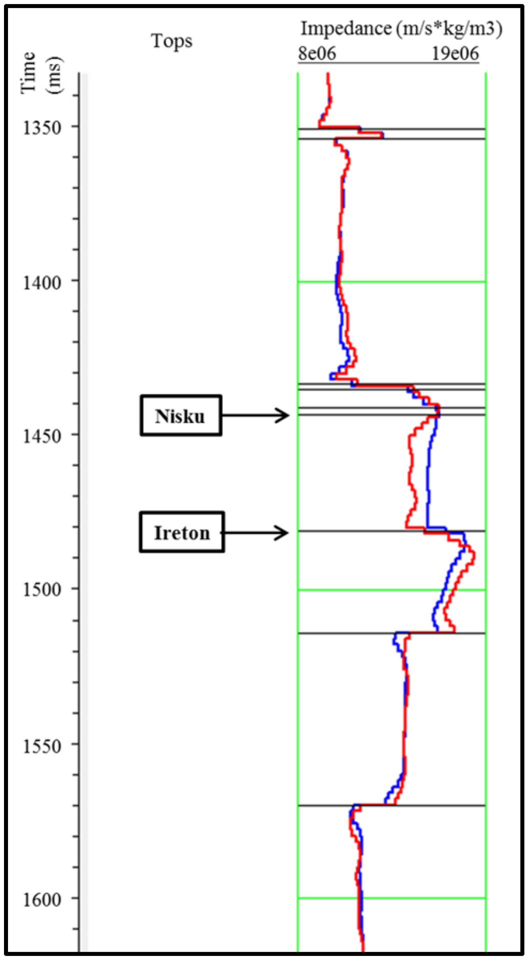

FIG. 32. Comparison of baseline (blue) and monitor (red) inverted traces at CDP location 726.

Similar to the differenced stacked sections, Figure 33 shows the effect within the injection zone determined from subtracting the monitor impedance section from the baseline impedance section. This difference represents the 100% CO_2 saturation zone. The traces outside the injection area were cancelled and only the injected region and reflectors below it are affected. The reflectors below the CO_2 plume are not as distorted as was seen in Figure 26. It is possible that the impedance changes in that region are not that significant so they were not resolved after the subtraction process. However, some artifacts are still present at the edges of the plume.

It is important to notice that these results identify the shape of the CO_2 plume even more clearly than just by directly comparing the differences in the seismic amplitudes. The top, base and sides of the plume are easily identifiable. The edges of the plume are again located between CDPs 702 and 752. Therefore, the width of the plume is accurately predicted from the inverted section difference (500 m).

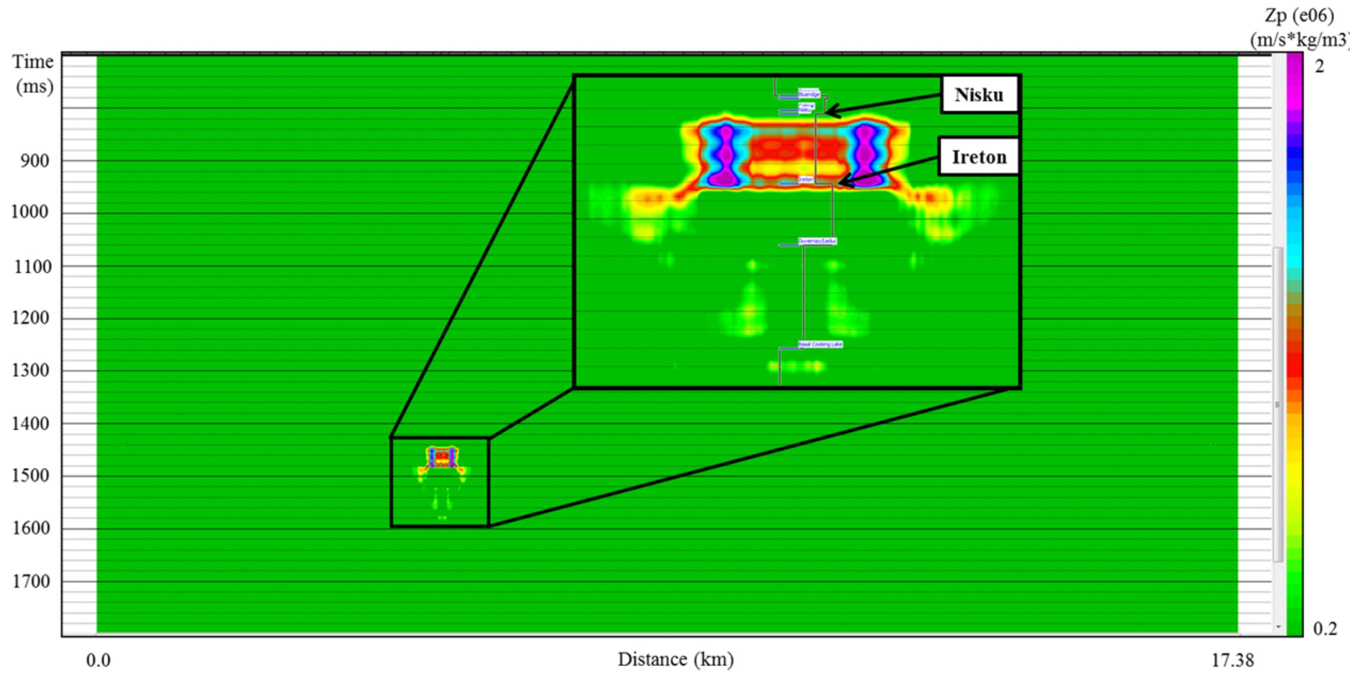

FIG. 33. Difference between baseline inversion and monitor inversion. The black square highlights 100% CO_2 injection zone.

A final test was undertaken to test the sensitivity of the inversion method by inverting the impedance difference rather than differencing the inversion of the monitor and baseline data. The difference of the CDP stacked sections (Figure 26) was taken into a model-based inversion analysis using as an initial model the impedance difference log. Therefore in this case just the effect of the CO_2 plume will contribute in the inversion study. Figure 34 shows the inversion analysis performed at the synthetic well location (CDP 726) in a window from 1400 ms to 1600 ms. The initial model was generated using the exact impedance values of the difference Zp log. P-impedance differences in the model range from 0 to almost 30×10^4 m/s*kg/m^3. The correlation between the synthetic (red) and the seismic trace (black) has a high correlation coefficient (0.98). The estimated RMS error between synthetic trace and the seismic trace is 0.22. The RMS error between the target log and the predicted log curves is 2.55×10^3 m/s*kg/m^3.

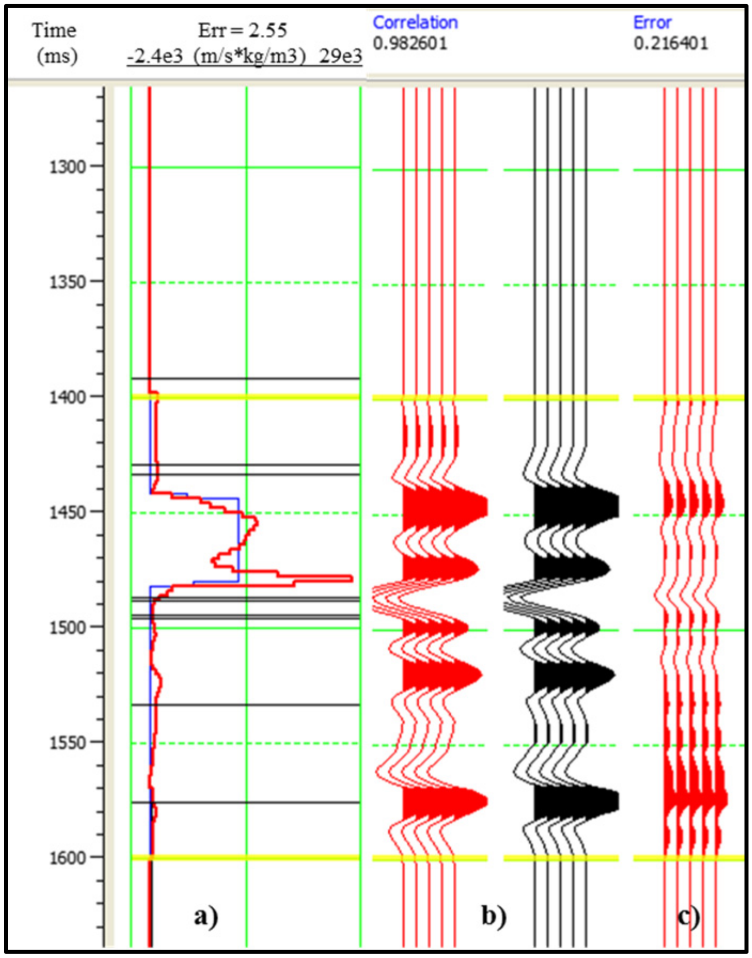

FIG. 34. Analysis of the post-stack inversion of the CDP stack section difference at synthetic well location: a) filtered impedance log (blue), initial model (black), inversion result (red); b) synthetic trace from inversion (red) and extracted trace from the seismic (black), and c) RMS error between synthetic trace and seismic trace.

In Figure 35 the result of the difference inversion is displayed in comparison with the difference of the independent inversions showed in Figure 33. Both look very similar but with different residual impedance values. These values are strongly related with the initial model that was used to run the inversion. Since Hampson-Russell inversion algorithm was developed to deal with full bandwidth seismic data, it is interesting to see that it performed quite well in the inversion of the difference.

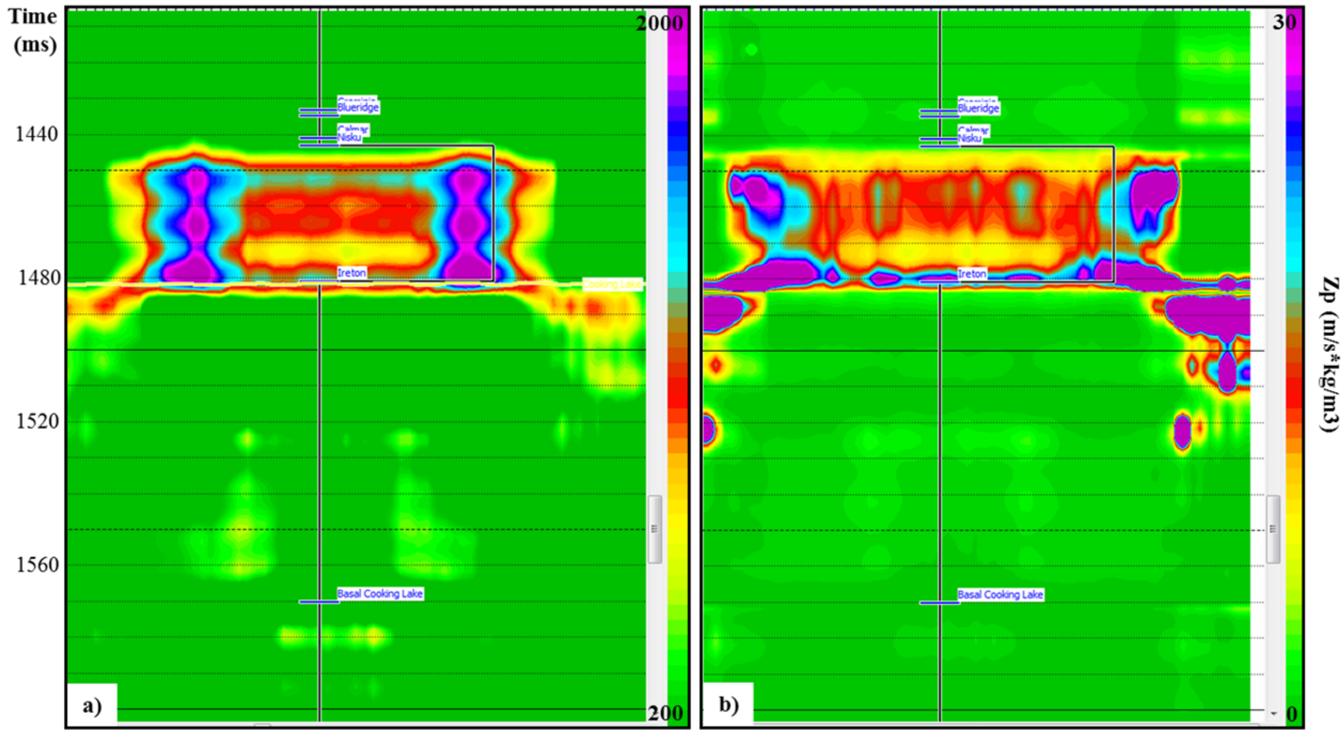

FIG. 35. a) Difference of impedance sections in Figure 31, b) inversion of the difference on Figure 26.

CONCLUSIONS

The objective of this project was to evaluate inversion of different datasets for studying the Nisku Formation.

Two seismic processing approaches applied to the same dataset were compared and tested in an inversion study. These approaches are based on a previously conditioned dataset with a conventional processing sequence (a) versus a new specialized processing sequence (b) focused on attaining coherent noise without compromising low-frequency signal. The conventional sequence used surface wave noise attenuation and spiking deconvolution processes, while the specialized sequence used radial filter and gabor deconvolution. The specialized processing flow resulted in better attenuation of low frequency noise while keeping the low frequency signal. In comparison with the previous processed stack, new result showed higher low frequency content around the target zone (from ~5-9 Hz) than the previous processing (from ~8-13 Hz), but showed a structural depression in the middle part of the section possibly related with a shallow channel caused by an old meander of the North Saskatchewan River. These frequency values were used to define the low-frequency initial inversion model.

A model-based inversion was performed in both datasets ((a) and (b)). In both cases, the inverted impedance showed good results at the well location and presented similar general trend and lateral variations. The inverted impedance in case b) showed a broadband result possibly related with the presence of more low frequency content in the seismic data. In case a) the result yielded a cleaner section possibly due to more powerful filters applied to the final stack and the units look more continuous without much lateral variation. Both results showed the Nisku Formation with lower values of impedance ($9x10^6$– $19x10^6$ m/s*kg/m^3) than those expected from the cross plot analysis (> $15x10^6$ m/s*kg/m^3); this could be associated with the higher porosity and permeability of this formation in comparison with the overlying formations plus the fluids present in the Nisku Formation (water and gas) which affect the impedance response.

The 2D seismic modelling undertaken in this study allowed us to simulate a CO_2 injection scenario within the Nisku saline aquifer. The post-injection seismic section shows a time delay of 1.8 ms of the basal reservoir reflector and amplitude change of ~30% with respect to the baseline case; and a decreased in the impedance values of ~7%. As expected, the impedance change is stronger due to the combination of Vp and ρ. The impedance changes of the reflectors underneath the plume are not significant and got cancelled after the subtraction process making easier the identification of the CO_2 plume. The shape of the plume was accurate estimated having a width of 500 m.

ACKNOWLEDGEMENTS

We thank TransAlta Corporation and Schlumberger for providing the data for this research. Special thanks to Shahin Moradi for her support with the 2D seismic modelling software, and to Brian Russell for useful discussions about inversion. Thank you to NORSAR-2D and Hampson-Russell (CGG) for providing the software used in this research. We also thank Carbon Management Canada (CMC), CREWES sponsors and members for financing and supporting this research.

REFERENCES

Alshuhail, A., 2011, CO2 Sequestration Site Characterization and Time-lapse Monitoring Using Reflection Seismic Methods: PhD. Thesis, Univ. of Calgary.

Carbon Management Canada, 2013, Retrieve September 22, 2013: http://www.cmc-nce.ca/events/gallery/

Chadwick A., R. Arts, O. Eiken, P. Williamson, and G. Williams., 2006, Geophysical Monitoring of the CO_2 Plume at Sleipner, North Sea: Advances in the Geological Storage of Carbon Dioxide, 303-314.

Dix, H. C., 1955, Seismic velocities from surface measurements: Geophysics, **20**, 68-86.

Frailey, S., 2009, Methods for Estimating CO2 Storage in Saline Aquifers: Elsevier Science Ltd. Energy, **1**, 2769-2776.

Gavotti, P. E and Lawton, D. C., 2013, Seismic processing workflow for supressing coherent noise while retaining low-frequency signal: CREWES Research Report, **25**.

Hampson-Russell., 2013, Hampson-Russell Assistant. Hampson-Russell Software Documentation. Hampson-Russell, a CGG Company.

Lindseth, R. O., 1979, Synthetic sonic logs – a process for stratigraphic interpretation: Geophysics, **44**, No. 1, 3-26.

Natural Resources Canada, 2013, Atlas of Canada - Alberta. Retrieved November 12, 2013, from Natural Resources Canada: http://atlas.nrcan.gc.ca/site/english/maps/reference/provincesterritories/alberta

Project Pioneer, 2013, Retrieve October 18, 2013: http://projectpioneer.ca/about-pioneer/maps

Sparlin, M., Meyer, J., Bevc, D., Cabrera, R., Hibbitts, T., and Rogers, J., 2010, Seismic analysis and characterization of a brine reservoir for CO_2 sequestration: 80th Ann. Internat. Mtg: Soc. of Expl. Geophys, 2304-2308.

TransAlta Corporation, 2013, Retrieve October 16, 2013: http://www.transalta.com/newsroom/feature-articles/2013-05-24/project-pioneer-publishes-its-final-report-pioneer-still-sharin

Vera, V. C., 2012, CO2 Seismic modelling of CO2 in a sandstone aquifer, Priddis, Alberta: M.Sc. Thesis, Univ. of Calgary.